MARTIN MARIETTA ENERGY SYSTEMS LIBRARIES

3 4456 0263008 0

ORNL/TM-10206/P1

ornl

OAK RIDGE NATIONAL LABORATORY

MARTIN MARIETTA

Procurement and Screening Test Data for Advanced Austenitic Alloys for 650°C Steam Service (Part 1, 14Cr-16Ni Steels and 20Cr-30Ni-Fe Alloys)

R. W. Swindeman
G. M. Goodwin
P. J. Maziasz

OAK RIDGE NATIONAL LABORATORY
CENTRAL RESEARCH LIBRARY
CIRCULATION SECTION
4500N ROOM 175
LIBRARY LOAN COPY
DO NOT TRANSFER TO ANOTHER PERSON
If you wish someone else to see this report, send in name with report and the library will arrange a loan.

Fossil Energy Progra

OPERATED BY
MARTIN MARIETTA ENERGY SYSTEMS, INC.
FOR THE UNITED STATES
DEPARTMENT OF ENERGY

Printed in the United States of America. Available from
National Technical Information Service
U.S. Department of Commerce
5285 Port Royal Road, Springfield, Virginia 22161
NTIS price codes—Printed Copy: A04 Microfiche A01

This report was prepared as an account of work sponsored by an agency of the United States Government. Neither the United States Government nor any agency thereof, nor any of their employees, makes any warranty, express or implied, or assumes any legal liability or responsibility for the accuracy, completeness, or usefulness of any information, apparatus, product, or process disclosed, or represents that its use would not infringe privately owned rights. Reference herein to any specific commercial product, process, or service by trade name, trademark, manufacturer, or otherwise, does not necessarily constitute or imply its endorsement, recommendation, or favoring by the United States Government or any agency thereof. The views and opinions of authors expressed herein do not necessarily state or reflect those of the United States Government or any agency thereof.

ORNL/TM-10206/P1

Metals and Ceramics Division

PROCUREMENT AND SCREENING TEST DATA FOR ADVANCED AUSTENITIC ALLOYS FOR 650°C STEAM SERVICE (PART 1, 14Cr-16Ni STEELS AND 20Cr-30Ni-Fe ALLOYS)

R. W. Swindeman, G. M. Goodwin, and P. J. Maziasz

Date Published: April 1987

Research sponsored by the
U.S. Department of Energy,
Advanced Research and Technology Development
Fossil Energy Materials Program

Prepared by the
OAK RIDGE NATIONAL LABORATORY
Oak Ridge, Tennessee 37831
operated by
MARTIN MARIETTA ENERGY SYSTEMS, INC.
for the
U.S. DEPARTMENT OF ENERGY
under contract DE-AC05-84OR21400

MARTIN MARIETTA ENERGY SYSTEMS LIBRARIES

3 4456 0263008 0

CONTENTS

ABSTRACT 1
INTRODUCTION 1
MATERIALS 2
COMMERCIAL ALLOYS 2
DEVELOPMENTAL ALLOYS 4
THERMAL-MECHANICAL TREATMENTS 5
FABRICABILITY 5
METALLURGICAL CHARACTERIZATION 7
WELDABILITY 11
MECHANICAL BEHAVIOR 16
TENSILE TESTING 16
CREEP-RUPTURE TESTING 20
LOW-STRESS CREEP TESTING 27
MICROSTRUCTURAL EXAMINATION 32
OPTICAL MICROSCOPY 32
EXTRACTION OF BULK PRECIPITATES 35
ANALYTICAL ELECTRON MICROSCOPY 41
DISCUSSION 53
RECOMMENDATIONS 54
ACKNOWLEDGMENTS 54
REFERENCES 54

PROCUREMENT AND SCREENING TEST DATA FOR ADVANCED AUSTENITIC ALLOYS FOR 650°C STEAM SERVICE (PART 1, 14Cr-16Ni STEELS AND 20Cr-30Ni-Fe ALLOYS)*

R. W. Swindeman, G. M. Goodwin, and P. J. Maziasz

ABSTRACT

Tests were initiated to evaluate the potential of a group of developmental iron-nickel-chromium alloys for service at 700°C with a target design stress of 60 MPa. Tensile, creep, stress rupture, weldability, and microstructural stability tests were conducted on one group of alloys, which are essentially modifications of type 316 stainless steel. The data for the alloys were compared to data for type 316 stainless steel, alloy 800H, and 17-14CuMo stainless steel. Results of the short-time screening tests indicate that the developmental alloys are superior to the commercial alloys in regard to strength. Annealing at 1115°C produced a loss in strength, but it was found that the loss could be mitigated by the judicious selection of composition, annealing conditions, and cold work prior to aging. The alloys were found to be unsatisfactory in regard to autogenous weldability; they exhibited a tendency for hot cracking. However, the steels could be joined satisfactorily with Inconel 82 and 17-14CuMo stainless steel filler metals. Compositions were identified that will be produced as small heats of tubing for subsequent fabricability, corrosion, and mechanical testing. Preliminary data relating to the fabricability and short-time mechanical properties were obtained for a second group of alloys. These were modifications of alloy 800H and contained molybdenum, niobium, and boron additions. Results indicated that significant improvement in strength is possible in the alloys containing 20% chromium and 30% nickel.

INTRODUCTION

This report contains the experimental results of a screening investigation to select a small group of austenitic alloys for evaluation as superheater/reheater tubing in advanced steam cycle applications. The rationale for such an undertaking and details of the program plan are contained in other reports.[1-4] The scope of the evaluation includes

*Research sponsored by the U.S. Department of Energy, AR&TD Fossil Energy Materials Program [DOE/FE AA 15 10 10 0, Work Breakdown Structure Elements ORNL-2(B), -2(C), and -2(D)] under contract DE-AC05-84OR21400 with Martin Marietta Energy Systems, Inc.

four groups of alloys based on type 316 stainless steel, type 310 stainless, alloy 800H, and aluminum-bearing iron-chromium-nickel alloys. It is expected that alloys containing less than 25% chromium will need to be chromized in order to allow adequate protection on the steam side at 650°C steam temperature. It is further expected that all alloys will need protection on the fire side because of the extremely corrosive nature of the liquid slag that forms on the tubing at temperatures in the range of 600 to 750°C.[3] Development of protective measures will follow the narrowing of candidate alloys to no more than sixteen.

An important aspect of the investigation is the requirement that it be directed to understanding materials and materials behavior and that it be representative of the scope of work funded through the Advanced Research and Technology Development (AR&TD) Fossil Energy Materials Program sponsored by the U.S. Department of Energy (DOE). To conform to this requirement, the investigation is focused on determining the underlying issues and problems and finding solutions related to the anticipated service of such materials, rather than on the production and commercialization of one specific candidate alloy.

This report describes the screening studies of modified 14Cr-16Ni stainless steel and some preliminary work on the modified 20Cr-30Ni alloys.

MATERIALS

The materials included in this report consist of 4 commercial alloys and 12 developmental alloys, which are identified in Table 1.

COMMERCIAL ALLOYS

The commercial alloys consisted of two heats of type 316 stainless steel pipe (250-mm diam by 64-mm wall), one heat of 17-14CuMo stainless steel bar (200-mm diam), and one plate of alloy 800H (13-mm thickness). One of the type 316 stainless pipes, identified here as ES1, was an archival remnant from material procured for the main steam line piping in the advanced-steam-cycle Eddystone plant operated by the Philadelphia Electric Company.[5] The alloy has seen approximately 20 years of service at temperatures in excess of 600°C. The second type 316 stainless steel pipe,

Table 1. Compositions of austenitic alloys

Alloy	Chemical analyses (wt %)																
	C	Si	Mn	Ni	Cr	Ti	Nb	V	Mo	P	B	S	N	Cu	Co	Other	Fe
316 ES1	0.059	0.56	1.79	13.18	16.49	<0.01	<0.01	0.02	2.24	0.013		0.020	0.043	0.09	0.10		Bal
316 ES2	0.064	0.54	1.78	13.20	16.44	<0.01	<0.01	0.02	2.24	0.013		0.021	0.042	0.09	0.10		Bal
800H	0.08	0.24	0.90	31.9	19.5	0.42						0.003		0.54		0.43Al	Bal
17-14CuMo	0.098	0.95	0.83	13.85	16.49	0.21	0.45	0.07	1.96	0.014		0.005	0.025	3.07	0.04		Bal
CE0 aim	0.08	0.4	2	16	14	0.3	0.1	0.5	2.5	0.07	0.007	0.02[a]	0.04[a]	0.2[a]			Bal
	0.072	0.41	1.80	16.0	14.2	0.24	0.10	0.57	2.45	0.071	0.005	0.007	0.015	0.03			
CE1 aim	0.08	0.1	2	16	14	0.3	0.1	0.5	2.5	0.07	0.007	0.02[a]	0.04[a]	0.2[a]			Bal
	0.085	0.21	1.64	16.2	13.1	0.21	0.12	0.52	2.30	0.076	0.005	0.008	0.016	0.04			
CE2 aim	0.08	0.1	2	16	16	0.3	0.1	0.5	2.5	0.07	0.007	0.02[a]	0.04[a]	0.2[a]			Bal
	0.079	0.26	1.89	16.0	16.1	0.31	0.11	0.58	2.26	0.069	0.005	0.008	0.017	0.03			
CE3 aim	0.08	0.1	2	16	14	0.3	0.1	0.5	2.5	0.07	0.007	0.02[a]	0.04[a]	2			Bal
	0.086	0.21	1.75	16.2	14.5	0.27	0.11	0.56	2.41	0.071	0.007	0.008	0.012	1.96			
AX7 aim	0.08	0.1	2	16	14	0.3	0.1	0.5	2.5	0.07	0.007	0.02[a]	0.04[a]	2			Bal
(P-3409)	0.073	0.11	2.00	16.0	14.2	0.18	0.15	0.53	2.48	0.073	0.005	0.014	0.024	1.5	0.009		Bal
AX5 aim	0.08	0.1	2	16	14	0.3	0.1	0.5	2.5	0.02	0.007	0.02[a]	0.04[a]	0.2[a]			Bal
(P-3407)	0.076	0.12	2.04	16.2	13.9	0.27	0.15	0.52	2.46	0.024	0.005	0.015	0.021	0.005	0.009		
AX6 aim	0.08	0.1	2	16	14	0.3	0.1	0.5	2.5	0.04	0.007	0.02[a]	0.04[a]	0.02[a]			Bal
(P-3408)	0.074	0.12	1.96	16.0	14.3	0.28	0.15	0.51	2.48	0.041	0.005	0.015	0.020	0.004	0.009		
AX8 aim	0.08	0.1	2	16	14	0.3	0.1	0.1	2.5	0.04	0.007	0.02[a]	0.04[a]	0.2[a]			Bal
(P-3410)	0.074	0.12	2.05	15.9	13.9	0.24	0.085	0.15	2.48	0.043	0.005	0.015	0.022	0.14	0.008		
AX1 aim	0.1	0.2	2	30	20	0.3	0.2	0.5	2	0.07	0.007	0.02[a]	0.04[a]				Bal
(P-3406)	0.087	0.20	1.99	29.8	19.6	0.27	0.21	0.52	1.98	0.074	0.005	0.012	0.003		0.008		
AX2 aim	0.1	0.2	2	30	20	0.3	0.2	0.5	2	0.04	0.007	0.02[a]	0.04[a]				Bal
(P-3402)	0.090	0.23	1.96	30.4	20.4	0.36	0.24	0.53	1.96	0.045	0.011	0.009	0.028		0.003		
AX3 aim	0.1	0.2	2	30	20	0.3	0.2	0.5	2	0.02	0.007	0.02[a]	0.04[a]				Bal
(P-3404)	0.092	0.22	2.00	30.6	20.6	0.36	0.24	0.52	2.00	0.031	0.010	0.010	0.029		0.008		
AX4 aim	0.1	0.2	2	30	25	0.3	0.2	0.5	2	0.07	0.007	0.02[a]	0.04[a]				Bal
(P-3404)	0.091	0.22	1.97	30.3	25.2	0.36	0.24	0.53	1.97	0.072	0.011	0.009	0.030		0.005		

[a]Maximum.

identified as ES2, was a remnant from replacement piping for Eddystone that proved to be unsuitable because of heat-affected-zone cracking that occured after a short time in service.[6]

The heat of alloy 800H was originally used for materials research in connection with the High Temperature Gas Cooled Reactor Program.[7]

The 17-14CuMo stainless steel was procured from Babcock and Wilcox and was originally intended for production of superheater/reheater tubing, for example, for the Eddystone plant.[5]

DEVELOPMENTAL ALLOYS

The chemical analyses of the commercial and developmental Combustion Engineering (CE) series of alloys are provided in Table 1. Alloy CE1 was the reference composition that was based on steels developed for irradiation resistance in nuclear applications. For application to superheater/reheater tubing, allowances were made for (1) increased nitrogen and silicon for ease of melting and (2) decreased phosphorus to improve hot fabricability and weldability.

Additional silicon was introduced to alloy CE0, and additional chromium was introduced to alloy CE2, to examine the influence of those elements on intermetallic-phase formation. Copper was added to alloy CE3 to examine its strengthening influence analogous to 17-14CuMo.

The compositions of alloys produced by AMAX Research Laboratory are provided in Table 1. These include alloys AX5 and AX6, similar to CE1 except for reduced phosphorus - 0.02% and 0.04% respectively; AX7, which is a repeat of CE3; and AX8, which contains reduced vanadium and phosphorus to examine the dependency of creep strength on these elements.

Four alloys that represent modifications of alloy 800H were produced by AMAX and are identified in Table 1. These alloys contain 20 to 25% chromium and 30% nickel. Other elemental additions were made similar to those introduced in the lean stainless steels, i.e., the CE series of alloys. The first three alloys (AX1, AX2, and AX3) represented an attempt to look at phosphorus effects in this class of alloys. The fourth alloy, AX4, had higher chromium content.

THERMAL-MECHANICAL TREATMENTS

The developmental alloys were examined under several conditions. First, tensile and creep-rupture tests were performed on mill-annealed (MA) material. This condition involved a solution treatment at 1200°C followed by rolling for flattening and final dimensioning by the mill. The mill processing produced varying amounts of cold or warm working. In the case of the AMAX alloys, the plates were finished with a 10% reduction in thickness by cold rolling. As expected, the yield strengths of the MA plates were substantially greater than those for the reannealed (RA) condition and were probably more representative of the condition of a tubing product that would require straightening, surface finishing, and dimensional control. The second treatment was a laboratory reanneal, which was performed on machined specimens (in groups of four) in vacuum. Two reannealing conditions were then examined – 0.5 h at 1115°C and 1 h at 1200°C. Next, the effect of laboratory-induced cold work was examined in some RA specimens. Two levels of cold work were introduced by tensile straining – nominally 2 and 5%. Finally, the alloys were heat treated by aging 24 h at 850°C and annealing 0.5 h at 1115°C. Because of the large number of variables and the limited material, not all alloys were examined under every condition.

FABRICABILITY

The fabrication sequence used by Combustion Engineering for the CE series of alloys is outlined in Fig. 1. Ingots (25 kg) were produced by argon-induction melting followed by electroslag remelting. The ingots were heated to 1200°C for 0.5 h and hot rolled, with approximately 10% reduction in thickness per pass and 1200°C anneals between passes. The finished thickness was 13 mm. All heats exhibited centerline delaminations in the rolled plates, starting at a location corresponding to the top of the original billet and moving toward the bottom. The material loss due to these defects was as follows: CE0, 40%; CE1, 10%; CE2, 40%; and CE3, 10%.

The AMAX alloys were vacuum-induction melted, poured as 20-kg ingots, and homogenized at 1250°C for 2 h. The anneals were performed at a minimum temperature of 1200°C and the rolling at 1100°C, with a 10% reduction

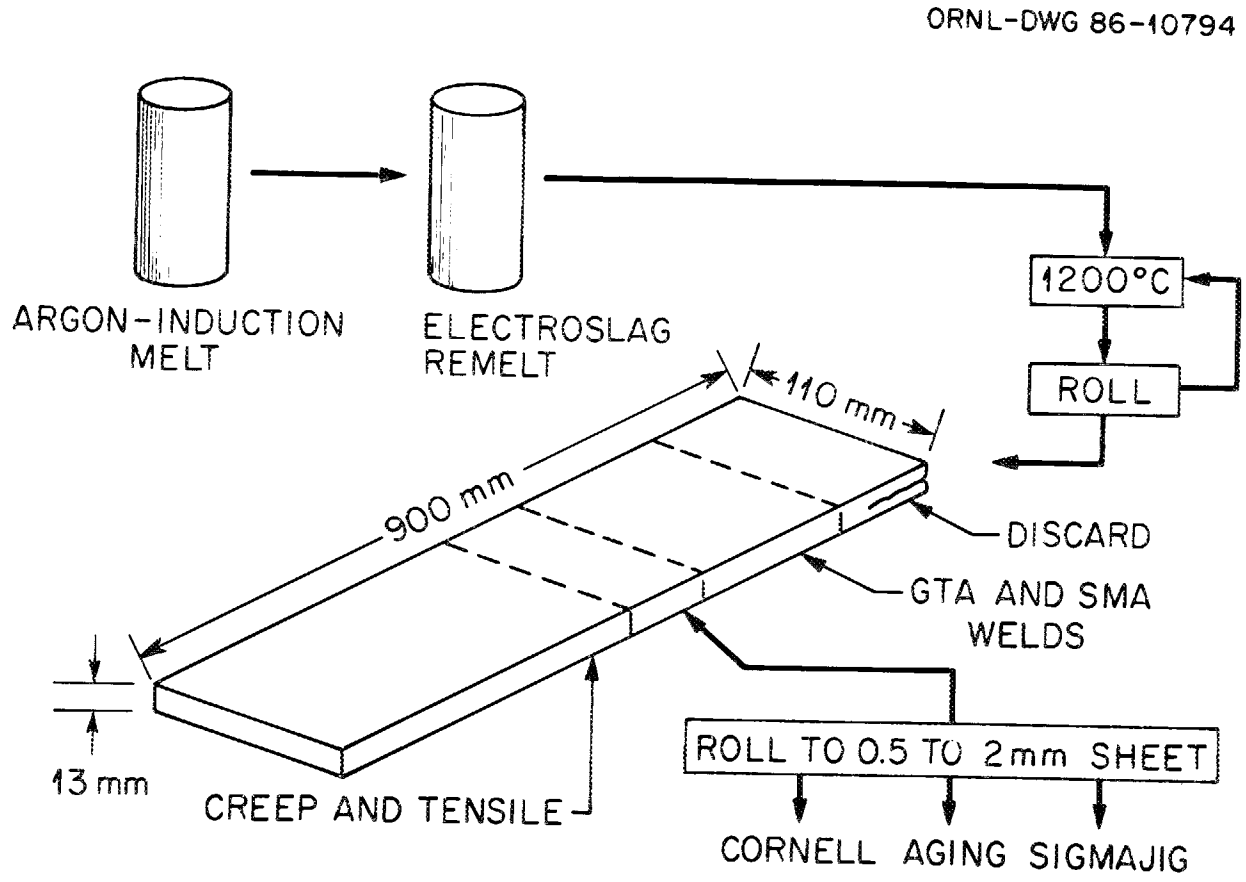

Fig. 1. Fabrication schedule for CE series of alloys.

in each pass. The alloys were finished by cold rolling. A typical as-received plate is shown in Fig. 2.

Further assessment of the fabricability of the alloys was obtained by rolling a portion of the 13-mm-thick plates at Oak Ridge National Laboratory (ORNL) to produce sheets that were needed for some types of mechanical testing. No problems were encountered when standard practices were used.

YP2223

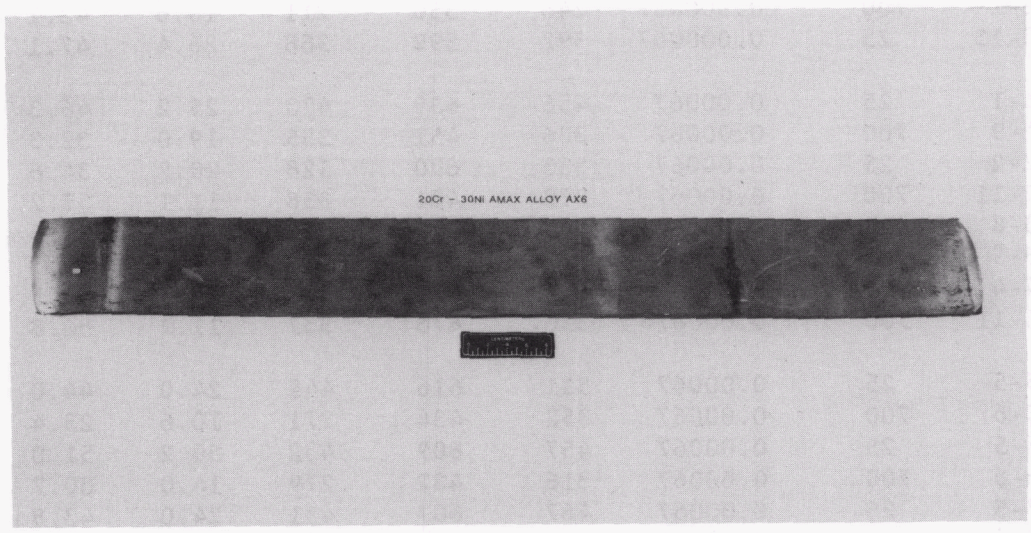

Fig. 2. Cold-rolled plate of 20Cr-30Ni developmental alloy AX6.

METALLURGICAL CHARACTERIZATION

Chemical analysis, tensile, metallography, and corrosion tests were conducted on the as-received alloys. Procedures generally followed those specified in ASTM A-240 for austenitic stainless steels.

With the exception of AMAX alloy AX7, which was low in titanium (0.18 vs 0.3 requested), the alloys met the required chemistries (Table 1).

Tensile tests at room temperature were performed on threaded-end test bars of standard configuration: 6.3-mm diam, 32-mm reduced length, and 25-mm test section. The nominal strain rate was 6.7×10^{-5} s^{-1} for the CE series of alloys and 6.7×10^{-4} s^{-1} for the AX series of alloys. Data are provided in Table 2, and tensile curves are shown in Fig. 3. Three of the

Table 2. Tensile data[a]

Specimen	Temperature (°C)	Rate (s^{-1})	0.2% YS (MPa)	UTS (MPa)	FS (MPa)	UE (%)	EL (%)	RA (%)
Mill-annealed condition								
CE0-5	25	0.000067	395	615	419	24.7	48.2	75.9
CE1-15	25	0.000067	231	561	362	34.5	58.0	76.5
CE1-17	700	0.000067	155	330	191	16.2	43.8	67.4
CE2-8	25	0.000067	402	628	436	27.1	61.0	75.3
CE2-1	700	0.000067	246	350	211	10.6	42.1	64.5
CE3-13	25	0.000067	392	592	368	26.4	47.1	77.1
AX1-1	25	0.00067	456	639	473	25.2	46.3	74.9
AX1-9	700	0.00067	306	451	355	19.0	32.3	42.3
AX2-2	25	0.00067	533	690	528	20.2	34.6	62.4
AX2-11	700	0.00067	378	481	338	11.1	37.2	56.0
AX3-8	25	0.00067	494	659	508	22.0	35.6	59.1
AX3-5	700	0.00067	347	473	338	15.6	39.5	53.9
AX4-4	25	0.00067	507	690	518	24.3	39.5	64.9
AX4-11	700	0.00067	330	478	337	11.7	36.8	56.6
AX5-5	25	0.00067	511	616	445	24.0	44.0	71.6
AX5-6	700	0.00067	352	434	271	10.6	25.4	62.4
AX6-5	25	0.00067	457	609	432	30.2	51.0	72.8
AX6-6	700	0.00067	316	432	279	14.0	30.7	62.1
AX7-5	25	0.00067	467	607	431	24.0	43.8	73.4
AX7-6	700	0.00067	319	431	299	13.9	30.0	56.4
AX8-5	25	0.00067	451	601	446	28.9	48.6	75.5
AX8-6	700	0.00067	313	419	264	14.7	31.7	53.6
CMO-26[b]	25	0.000067	250	541	476	36.7	52.3	54.5
CMO-25[b]	700	0.000067	157	299	218	13.1	31.2	31.1
1115°C reannealed condition								
CE0-8	25	0.000067	228	580	392	31.1	56.1	75.0
CE1-13	25	0.000067	213	565	342	29.2	55.6	75.0
CE2-9	25	0.000067	225	585	387	36.9	47.7	75.4
CE2-4	700	0.000067	149	323	161	19.0	51.9	67.3
CE3-9	25	0.000067	222	567	365	32.6	55.1	74.0
1200°C reannealed condition								
CE1-18	25	0.000067	175	551	366	54.9	72.3	75.1
CE1-11	700	0.000067	123	359	187	25.4	26.3	45.8
CE2-7	700	0.000067	120	345	211	24.8	38.2	43.0

[a]YS = yield strength, UTS = ultimate tensile strength, FS = fracture strength, UE = uniform elongation, EL = elongation in 4 × diameter, RA = reduction of area.

[b]CMO = 17-14CuMo stainless steel.

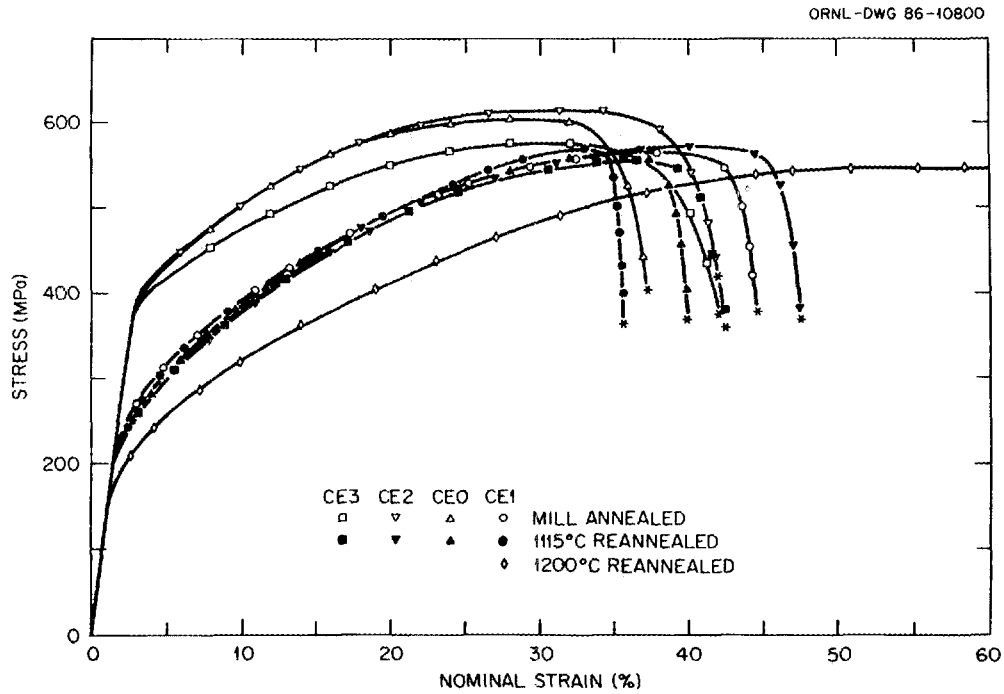

Fig. 3. Room-temperature tensile curves for CE series alloys.

CE series alloys, processed together, exhibited very similar tensile curves, with yield strengths in excess of 300 MPa and ultimate strengths greater than 550 MPa. The first alloy processed by CE (CE1) was weaker than the others but exceeded the minimum tensile requirements of ASTM A-240 by a wide margin. The AMAX series of alloys were generally stronger but less ductile than the CE alloys in the mill-annealed condition. All alloys exhibited satisfactory ductility. Tensile data for 17-14CuMo steel are included in Table 1 for comparison.

Photomicrographs of the CE alloys are shown in Fig. 4. The MA microstructures indicate that the medium grain sizes and the elongation of the grains in the rolling direction are consistent with approximately 10% cold or hot work. The inclusion density was low, with only a few stringers widely separated. Cubic particles, probably titanium nitride, were interspersed throughout the microstructure. The microstructures for specimens reannealed at 1115°C revealed smaller grain sizes, indicating that sufficient cold work was in the alloys to produce recrystallization during annealing.

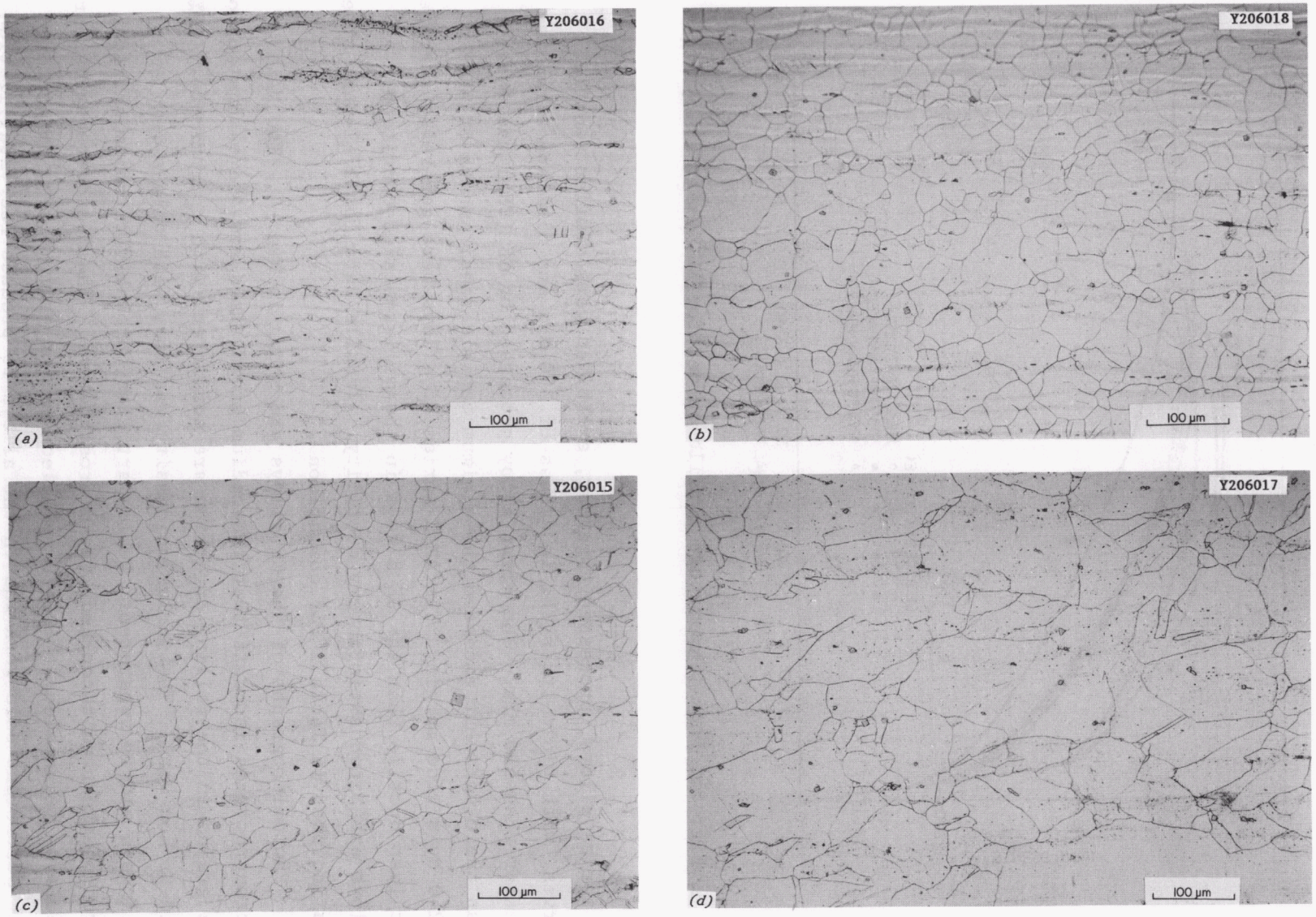

Fig. 4. Microstructures of mill annealed CE alloy series. (*a*) Heat CE0. (*b*) Heat CE1. (*c*) Heat CE2. (*d*) Heat CE3.

WELDABILITY

Weldability experiments were performed on the commercial and developmental alloys. The primary concern with regard to the developmental alloys is the likelihood of hot cracking due to the high phosphorus contents. To examine this likehood, experiments were conducted on sheet specimens using a newly developed device called a Sigmajig[8] (see Fig. 5). The Sigmajig consists of a steel frame that supports a copper chill block, which is placed in position to contact a 50- × 50-mm square sheet specimen, and clamping steel plates used to grip opposite edges of the specimen. One of the clamps is movable and is designed to impose a stress on the sheet prior to welding by means of bolts that join the movable plate to the steel frame and then pass through a column of spring washers. The stress is maintained during the welding process by the high compliance of the column of spring washers. Changes in the stress during the welding are monitored by strain gages placed in the bolts. The autogenous gas tungsten arc (GTA) welding process is used for the evaluation.

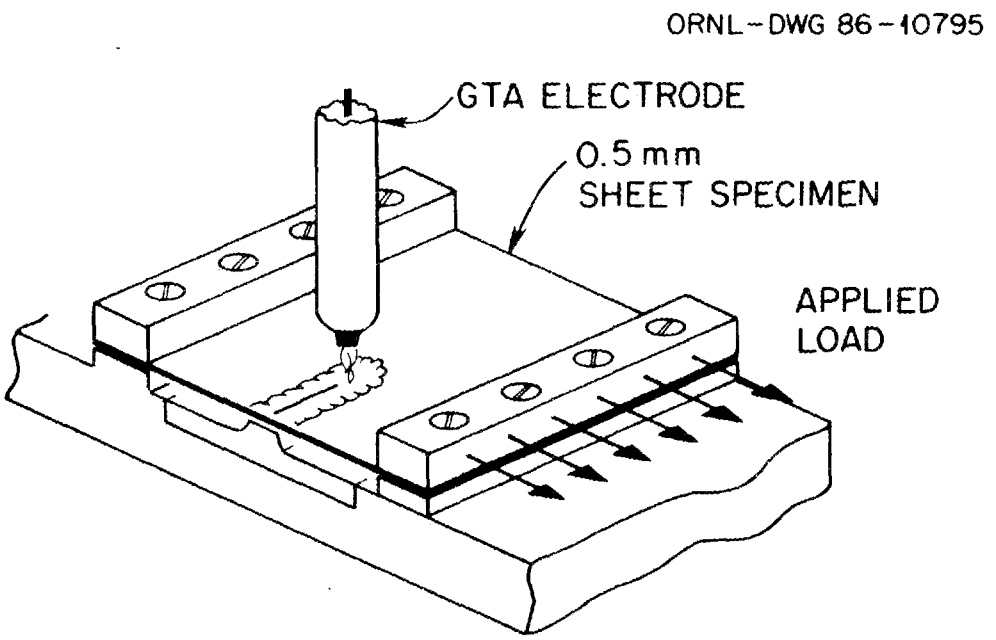

Fig. 5. Schematic drawing of the experimental fixturing of the Sigmajig test to evaluate hot-cracking tendency.

To determine the weldability of the steels, a series of tests on sheets of identical thickness is performed in which the stress is increased incrementally, from one test specimen to the next, followed by measurement of the percent of fusion zone cracking. Figure 6 shows the results of a typical test. The percent cracking is then plotted against the applied stress, as shown in Fig. 7 for the CE series of developmental alloys, 17-14CuMo stainless steel, and the scatterband associated with 15 heats of types 304 and 316 stainless steel. Those heats that can be welded without hot-cracking problems lie to the right of the plot and can withstand applied stresses on the order of the room-temperature yield strength. Qualitatively, the results in Fig. 7 indicate that the developmental alloys are susceptible to hot cracking. None of the alloys can match 17-14CuMo steel, which is marginal compared with type 316 stainless steel. However, these results do not indicate that the steels cannot be joined but rather that other filler metals, preferably those that contain reduced phosphorus, must be used.

Welds were produced in plates of CE series alloys using Inconel 82 (ERNiCr3) and 17-14CuMo stainless steel filler metals. The Inconel 82 filler metal was used to produce a manual GTA weld in 13-mm-thick heat CE2, fully restrained on a type 316 stainless steel plate. The welding conditions were as follows:

Current:	155 A, direct current straight polarity (DCSP)
Filler wire:	2.4-mm (3/32-in.) diam.
Number of passes:	12

The weldment passed the side-bend test per ASME Sect. IX. In a room-temperature tensile test the weldment failed in the base metal well away from the fusion line. At 700°C, failure occurred at the weld centerline and a few small fissures appeared at the fusion line. A creep-rupture test was performed at 700°C and 170 MPa. The specimen failed in the center of the weld after 771 h.

A GTA weld was produced in CE1 using braided 17-14CuMo stainless steel wire. Again, the 13-mm plate was fully restrained on a type 316 stainless steel backing plate, as shown in Fig. 8. Welding conditions were as follows:

M29919

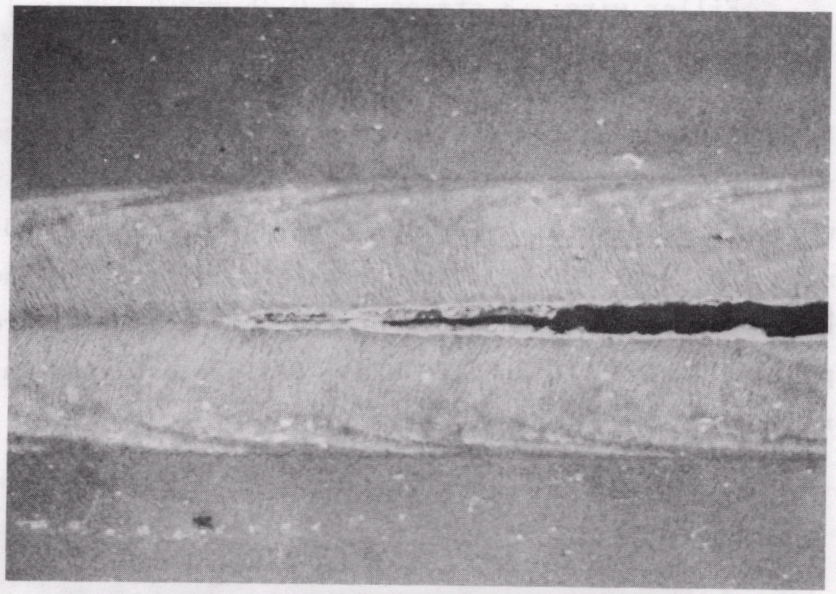

Fig. 6. Typical hot crack produced in the Sigmajig.

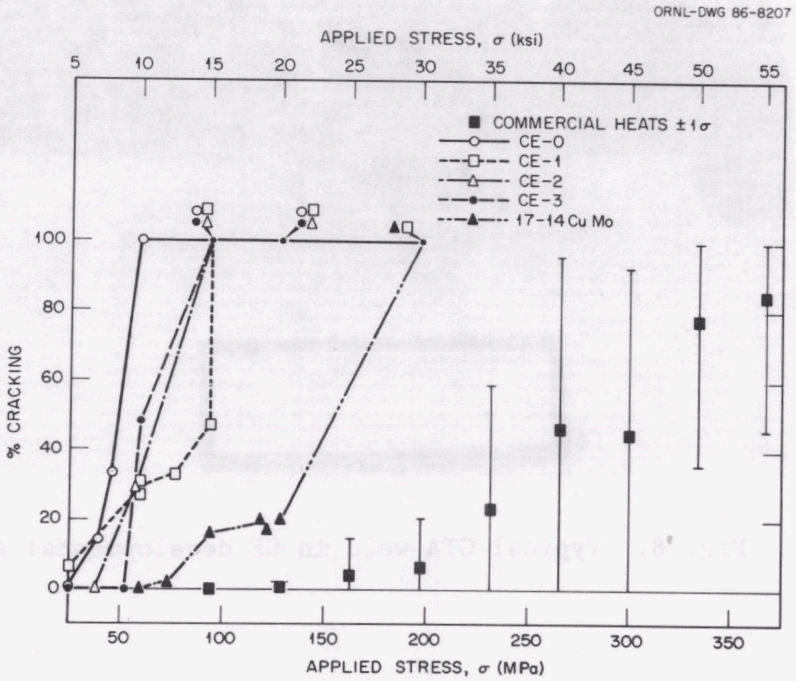

Fig. 7. Comparison of hot cracking tendency of CE series alloys with that of 17-14CuMo and commerical heats of type 316 stainless steel.

Current: 170 A, DCSP

Filler wire: 8 strands of 0.76-mm (0.030-in.) twisted

Number of passes: 8

The weldment heat-affected zone passed the side-bend test, but several small fissures appeared near the fusion line at the toe and the crown in the weld metal. Tensile test data (see Table 3) show reduced strength and ductility relative to base metal and the Inconel 82 weld. Failures occurred in the center of the weld metal. A creep rupture test was performed at 700°C and 170 MPa. Failure occurred in the weld metal after 863 h.

YP1909

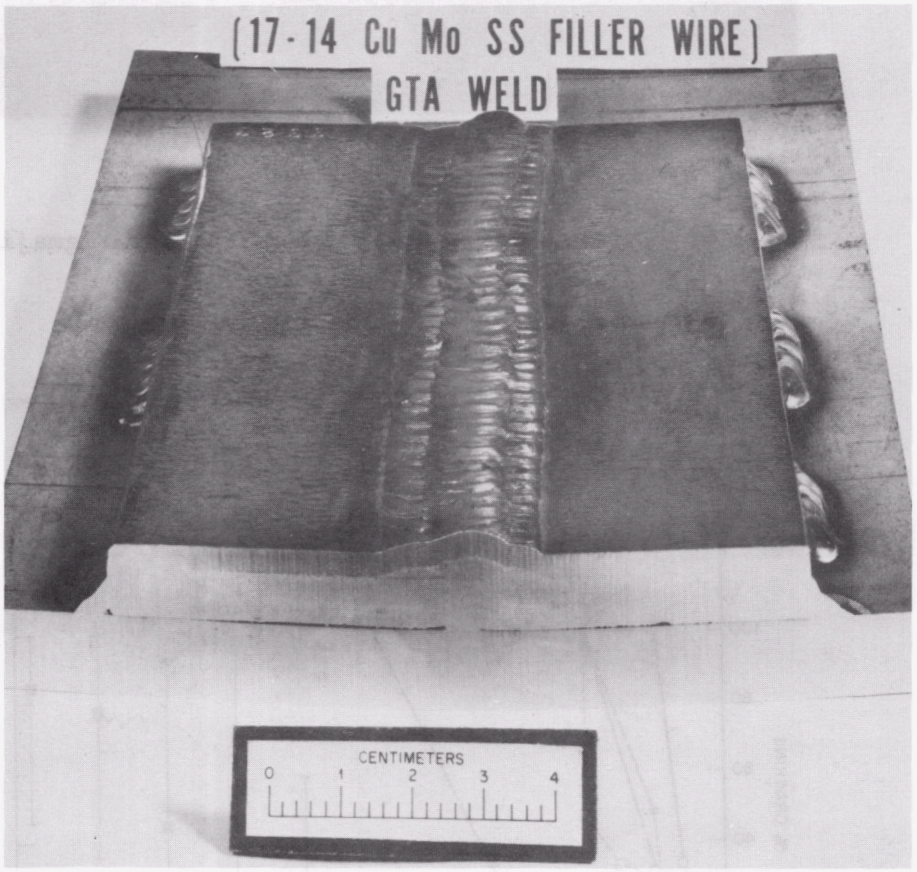

Fig. 8. Typical GTA weld in CE developmental alloy.

Table 3. Tensile data[a] for weldments

Specimen	Temperature (°C)	Rate (s^{-1})	0.2% YS (MPa)	UTS (MPa)	FS (MP)	UE (%)	EL (%)	RA (%)
GTA Inconel 82 weld tensile data								
CEW1	25	0.000067	351	594	385	31.0	55	72.5
CEW3	700	0.000067	266	327	114	6.2	41.5	68.4
GTA 17-14CuMo weld tensile data								
CEW7	25	0.000067	293	513	418	12.5	15.0	32.8
CEW8	25	0.000067	284	518	141	12.5	12.1	30.6
CEW5	700	0.000067	211	331	212	6.0	11.0	22.6
SMA 17-14CuMo weld tensile data								
CEW12	25	0.000067	283	612	502	27.2	51.4	72.9
CEW9	700	0.000067	208	341	202	11.5	40.1	72.7

[a]YS = yield strength, UTS = ultimate tensile strength, FS = fracture strength, UE = uniform elongation, EL = elongation in 4 × diameter, RA = reduction of area.

A shielded metal arc (SMA) weld was produced in a 13-mm-thick plate of CE1 using an E17-14CrMo stainless steel electrode. The welding conditions were as follows:

Current: 90 A, DCRP
Voltage: 30
Filler metal: 3.2-mm-diam (1/8-in.) electrode
Number of passes: 12

The weldment passed the side bend test with no indication of hot cracking. The tensile data are reported in Table 3. At room temperature, the specimen broke in the base metal, well away from the fusion line. At 700°C, failure occurred in the center of the weld metal. A creep rupture test at 700°C and 170 MPa produced failure in the base metal after 1758 h.

In summary, results of the screening tests on weldability for the CE alloy series show that the steels can be joined with suitable filler metals but that the potential for hot cracking exists in the region of the fusion line. Weld cycle simulations by means of the Gleeble machine are needed to examine the extent of the problem and to fix upper limits on phosphorus and minor element additions.

MECHANICAL BEHAVIOR

The mechanical tests performed on the commercial and developmental heats consisted of tensile, creep-rupture, and variable-stress creep tests designed to examine hardening and recovery behavior as a function of composition, heat treatment, and strain history. In addition, a series of tensile tests on smaller sheet tensile specimens was run on several alloys in the solution-annealed (1 h at 1120°C) condition (alloys 800H, 17-14CuMo, and CE1) and in the 25% cold-worked condition (CE1) at 25 to 800°C. The screening test matrix for creep rupture was developed with the understanding that the results would be complemented by relaxation data produced at Cornell University under a related AR&TD subcontract. Thus, the constant-load creep rupture test at ORNL allows one to examine the influence of accumulated creep strain on subsequent strain rate, while relaxation tests at Cornell allow one to determine the influence of stress on strain rate at essentially constant strain.

TENSILE TESTING

The results from tensile tests at 25 and 700°C are provided in Tables 2 and 4 for the CE series alloys, some of the AMAX series alloys, and 17-14CuMo stainless steel; representative curves for the CE series alloys at 25°C are plotted in Fig. 3. Figure 3 shows that the MA material is the strongest in regard to yield strength, followed by the 1115°C RA and then the 1200°C RA. The CE series alloys processed together by

Combustion Engineering (CE0, CE2, and CE3) were of similar strength, while CE1 came closest to matching the strength of the 1115°C material. The CE series alloys that were reannealed at 1200°C did not meet the 207-MPa minimum yield strength required for H-grade stainless steels in ASTM A-240. Although this is a concern, it should be realized that laboratory RA specimens of most 300-series stainless steels fail to meet this requirement. Flattening or straightening of mill products usually produces enough cold work to meet the minimum strength.

Representative tensile curves for the CE alloy at 700°C are provided in Fig. 9. These show significant differences between the MA, 1115°C RA, and 1200°C RA conditions. This 1200°C RA material, which was weak at 25°C, exhibits an acceptable yield strength at 700°C and has an ultimate strength equivalent to that of the MA condition. The 1115°C RA produced the best high-temperature elongation but also a lower ultimate strength than the MA and 1200°C RA treatments.

Tensile data on the sheet specimens tested from 25 to 800°C are given in Table 4; strength and elongation as functions of temperature are plotted in Fig. 10(*a*). The data on CE1 from this set of data on material reannealed at 1120°C are comparable to that obtained on the larger specimens of the same steel reannealed at 1115°C. Room-temperature tests were run in air, but higher-temperature testing was done in vacuum.

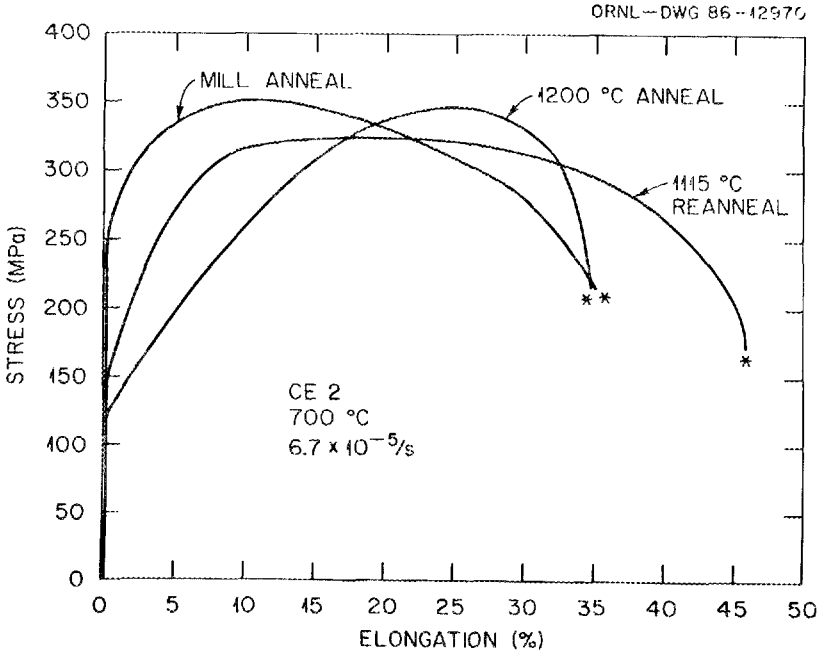

Fig. 9. Effect of annealing on the tensile curve at 700°C.

Table 4. Tensile properties of alloys as a function of temperature

Alloy	Specimen	Test temperature (°C)	Strength (MPa)		Elongation (%)	
			Yield	Ultimate	Uniform	Total
		Solution annealed				
800H	8H-06	25	181	545	36.8	40
	8H-08	25	157	525	38.9	41.9
	8H-02	600	91	439	40.1	42.8
	8H-07	600	87	426	38.4	40.9
	8H-03	700	86	311	26.4	35.8
	8H-01	700	83	308	26.1	35.1
	8H-04	750	83	238	16.9	34.6
	8H-05	750	86	242	17.6	31.8
17-14CuMo	CM-01	25	188	554	40.9	44.4
	CM-38	25	185	547	38.6	43.6
	CM-17	200	173	498	32.4	36.9
	CM-16	200	177	509	31.5	36
	CM-02	400	114	454	33.6	34.4
	CM-06	400	124	477	30	32.5
	CM-33	500	115	487	31.9	34.6
	CM-19	500	111	462	28.6	34
	CM-08	600	109	452	28.5	31.6
	CM-11	600	109	448	27.8	30.8
	CM-12	700	107	339	21.5	28.6
	CM-23	700	103	331	21.4	29.1
	CM-35	750	101	264	15	25.5
	CM-34	750	104	269	15.5	25.9
	CM-04	800	114	213	12	25.3
	CM-39	800	103	191	12.6	24.5
CE1	CA-41	25	206	565	38.9	44
	CA-28	25	189	553	68	71.4
	CA-13	200	151	473	40.9	44.8
	CA-34	200	162	466	41.2	45.8
	CA-16	400	93	429	39.6	42.4
	CA-19	400	95	430	38.1	40.3
	CA-37	500	85	436	38.5	43
	CA-02	500	81	418	37.9	40.1
	CA-21	600	81	399	36.3	39.1
	CA-11	600	81	401	35.1	39
	CA-13	700	68	273	25.3	28.5
	CA-17	700	68	270	25.1	28.8
	CA-06	750	68	212	19.4	25.6
	CA-09	750	62	210	20.6	28.3
	CA-01	800	65	169	16.8	31.3
	CA-27	800	70	172	17	31.9
		25% Cold worked				
CE1	CW-13	25	739	789	6.5	9.5
	CW-37	25	717	748	7.5	10.9
	CW-02	200	700	731	2.3	6.0
	CW-05	200	730	778	1.6	5.3
	CW-08	400	642	684	0.8	2.1
	CW-36	400	599	633	1.1	3.0
	CW-04	500	572	629	1.5	3.1
	CW-21	500	586	625	1.4	3
	CW-10	600	550	601	1.8	3.4
	CW-26	600	540	584	1.5	3.1
	CW-09	700	442	474	2.1	4.6
	CW-11	700	413	448	2.3	4.6
	CW-35	750	341	360	1.5	5.6
	CW-14	750	335	346	1.1	5
	CW-12	800	364	272	1.0	7.4
	CW-16	800	278	286	1.0	7.1

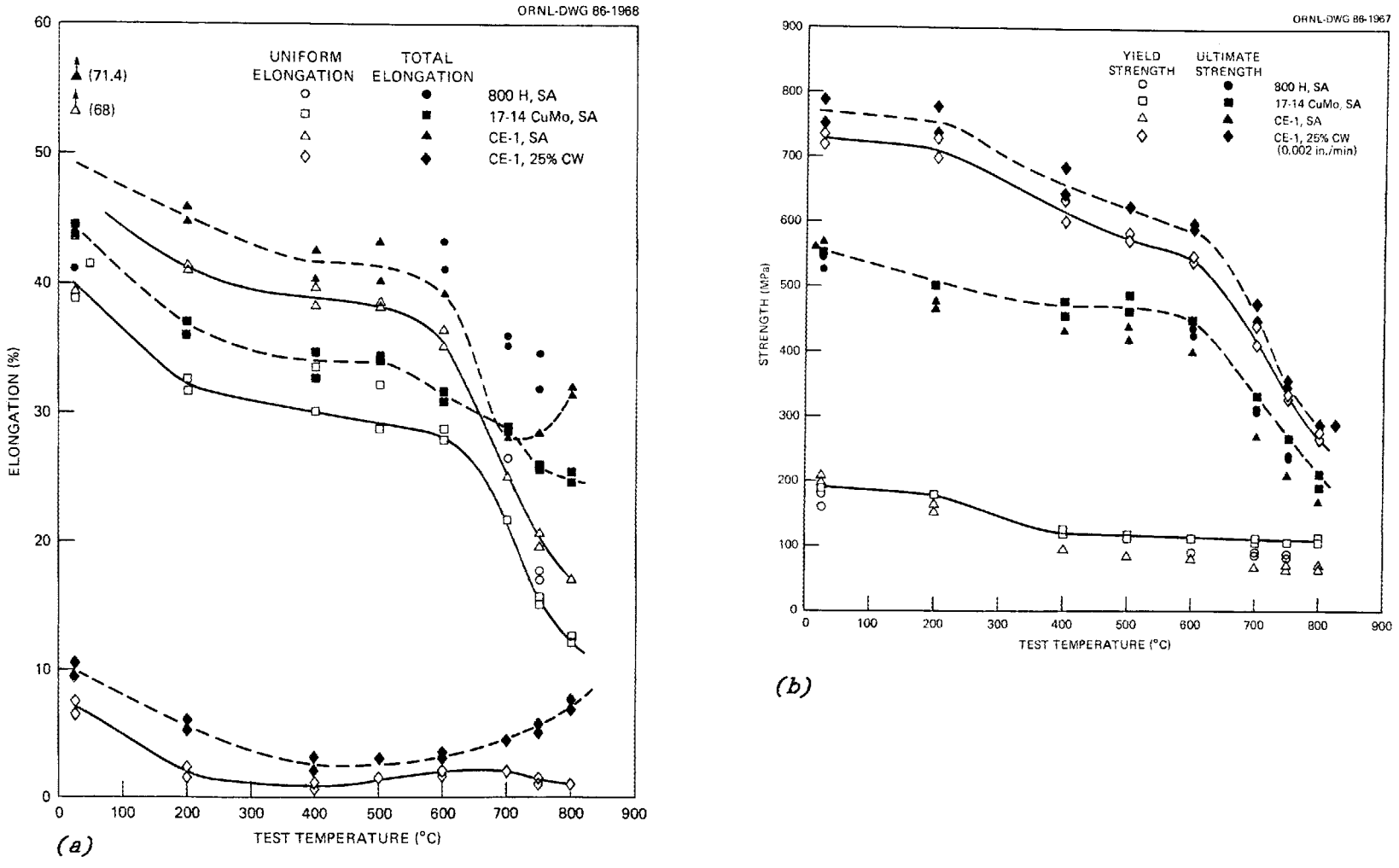

Fig. 10. Effect of temperature on the tensile properties of alloy 800H, 17-14CuMo stainless steel, and alloy CE1 in the solution annealed condition and in the solution annealed plus 25% cold worked condition.

For the RA alloys, the 17-14CuMo was somewhat stronger while CE1 was weaker, particularly at 400°C and above. The various alloys also showed similar strength dependencies on test temperature. The greatest decrease in yield strength occurred from 25 to 400°C; above 400°C, yield strength either stayed constant (17-14CuMo) or decreased slightly with increased temperature. Ultimate strength declined slightly as temperatures rose from 25 to 600°C but then dropped more sharply with temperatures above 600°C.

All of the RA alloys showed ductilities at or above 30% up to 600°C, with CE1 being more ductile than 17-14CuMo and similar to 800H; this is consistent with the strength properties. Uniform elongation declined sharply with temperatures above 600°C. This was particularly true for alloy 800H. Total elongation declined more gradually for 800H and 17-14CuMo above 600°C but dropped to a minimum at 700°C and then increased with temperature for CE1. Ductility was much lower for the 25% cold worked (CW) CE1, as would be expected considering the greater strength of this alloy. Elongations were at a minimum at 400°C and then increased up to 700°C. Total elongation continued to increase above 700°C, but uniform elongation decreased. The uniform elongation was quite low from 200 to 800°C for the 25% CW CE1, often being near 1%.

CREEP-RUPTURE TESTING

Approximately 40 creep-rupture tests were performed. The first series of tests was aimed at comparing the creep behavior of the MA alloys with that of the commercial alloys at a single temperature and stress. The reference testing was conducted at 700°C and a stress of 170 MPa. Figure 11 shows a comparison of the creep curves produced by this series of tests. For alloys in the MA condition, the Eddystone archive heat of 316 stainless steel (ES1) failed in 12 h; alloy 800H failed in 118 h; 17-14CuMo stainless steel failed in 1400 h; and the CE series alloys CE0, CE1, CE2, and CE3 failed in >6174, 1432, 2365, and 4940 h, respectively. Tests of the AMAX series of 14Cr-16Ni alloys in the MA condition accumulated 3000 h with less than 1% creep strain. The initial test data provided sufficient encouragement to continue with the screening tests on the CE series of developmental alloys. The test matrix and the results

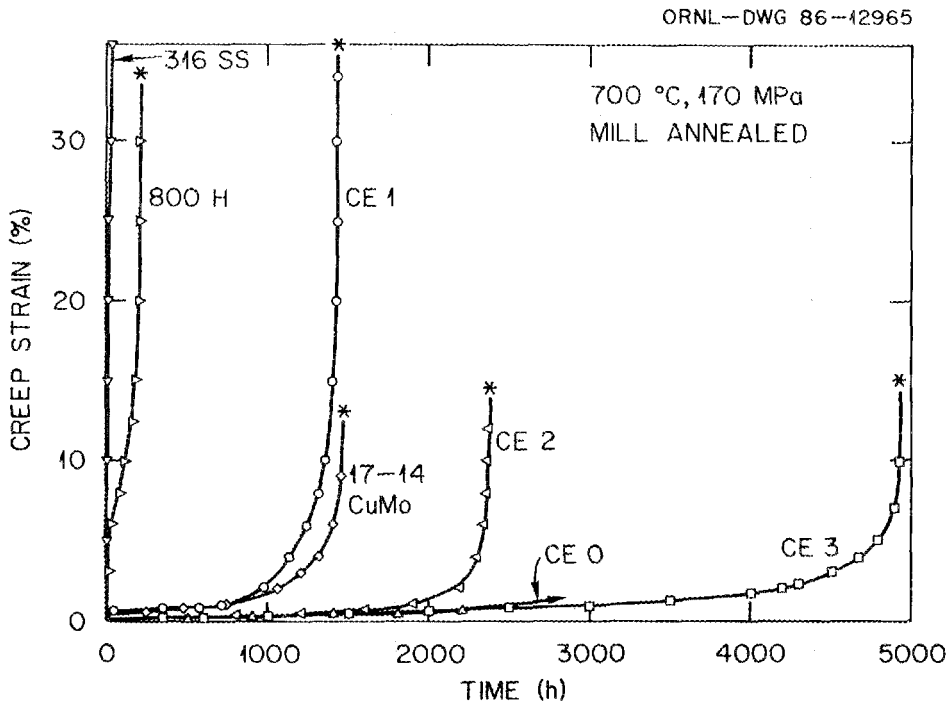

Fig. 11. Comparison of creep curves at 700°C and 170 MPa.

corresponding to the time to 1% creep and rupture life for these alloys are provided in Tables 5 and 6. All data are from tests at 700°C and 170 MPa. The effect of reannealing temperature was first examined. The 1115°C RA produced a loss in the times to 1% creep and rupture relative to the MA condition. Only CE0, CE2, and CE3 were tested, but all were similar. Next, all four CE and AMAX 14Cr-16Ni series alloys were tested in the 1200°C RA condition. For the CE alloys the times to 1% creep and rupture were longer than those for the 1115°C RA. Figure 12 shows these trends.

The next test series examined the effect of aging at 850°C for 24 h. Comparisons were made for the CE2 and CE3 alloys in the MA vs the MA plus aged condition, the CE0 alloy for the 1115°C RA plus cold-work and aged condition, and the CE2 alloy for the 1200°C RA vs the 1200°C RA plus aged condition. The aging reduced the life for all starting conditions. However, the MA specimens were the least affected and the 1115°C RA specimens were the most affected. Representative creep curves showing the aging effect are provided in Fig. 12.

Table 5. Effect of annealing temperature, cold work, and aging on the time to 1% creep for CE series alloys at 700°C and 170 MPa

Alloy	Time to 1% creep (h)					
	Mill anneal	1115°C anneal			1200°C anneal	
		0% CW[a]	2% CW	5% CW	0% CW	5% CW
CE0	3200	700	1200	1000	2300	4400
CE1	730				2300	>3100
CE2	1910	900			1950	
CE3	2900	900			2300	
Aged at 850°C for 24 h						
CE0		4	7	206		
CE2	2750				550	
CE3	2200					

[a]CW = cold work.

Table 6. Effect of annealing temperature, cold work, and aging on the time to rupture for CE series alloys at 700°C and 170 MPa

Alloy	Time to rupture (h)					
	Mill anneal	1115°C anneal			1200°C anneal	
		0% CW[a]	2% CW	5% CW	0% CW	5% CW
CE0	6174		1722	1519	5098	>5000
CE1	1432				3728	3100
CE2	2365	1415			2714	
CE3	4940	1391			>3200	
Aged at 850°C for 24 h						
CE0		238	184	502		
CE2	>4000				771	
CE3	3795					

[a]CW = cold work.

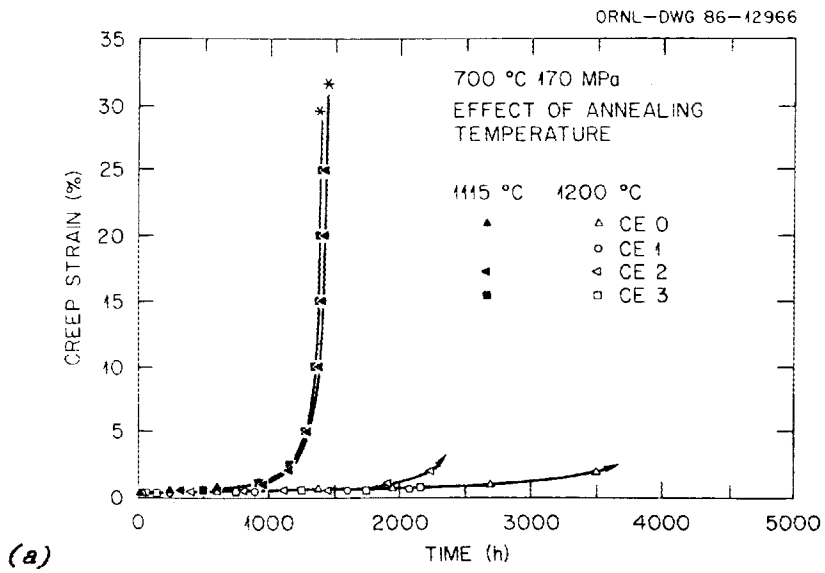

(a)

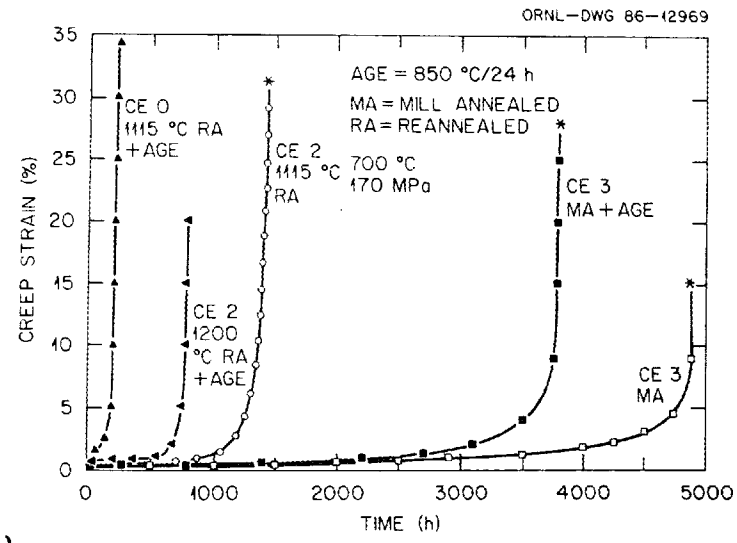

(b)

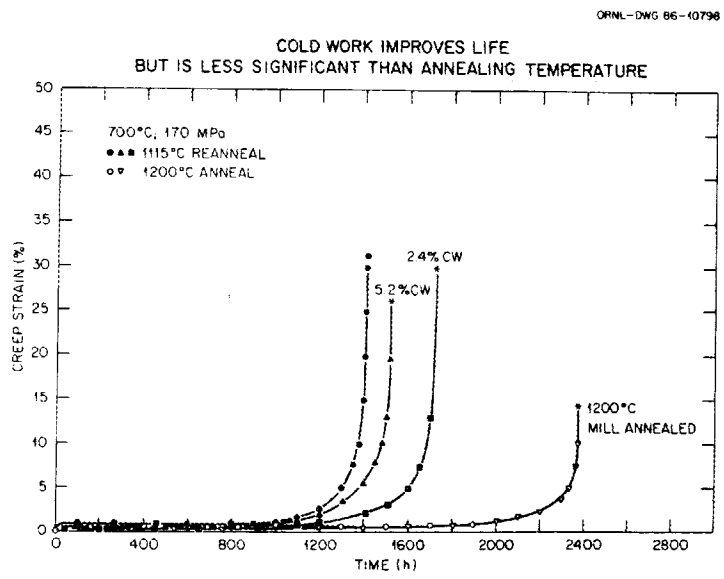

(c)

Fig. 12. Effect of (*a*) annealing temperature, (*b*) aging, and (*c*) cold work on creep at 700°C and 170 MPa.

Cold-working effects were examined in the CE0 alloy, but tests are continuing. Trends suggest that cold work increases the time to 1% creep but does not produce large differences in the time to rupture. Some comparisons of creep curves are provided in Fig. 12.

In summary, the screening tests indicated that the annealing temperature for the CE series alloys should be in the vicinity of 1200°C and that modest amounts of cold work can not only be tolerated but can be beneficial. Insufficient data have been collected to establish recommendations for heat treating the AMAX alloys with high chromium and nickel.

The CE3 alloy was selected for more extensive studies of the influence of stress and temperature on creep behavior for two reasons. First, more material was available; second, the alloy had good strength in the MA condition. Data gathered on this alloy are summarized in Figs. 13 and 14. Figure 13 shows a plot of stress vs the time to 1% creep strain. The lines in the figure represent the fit of the data to the following model:

$$1/t = (S/a)^n \exp(S/v) \exp(-Q/T) \quad , \qquad (1)$$

where t is time (h) to 1% creep; S is stress (MPa); T is temperature (K); and a, v, and Q are material parameters. Extrapolation to 100,000 h at 700°C by means of the model indicates that the stress will be well in excess of the target strength (100 MPa). The stress vs time-to-rupture data are provided in Fig. 14. A model similar to Eq. (1) is represented by the lines through the data. Again, extrapolation by means of the model suggests that the target strength[3,4] (100 MPa) at 100,000 h and 700°C could be met by heat CE3 in the MA condition. The time to 1% creep is ~70% of the time to rupture, as indicated in Fig. 15.

A comparison of the creep-rupture strength with other alloys is provided in Fig. 16, where a comparison is made between data for CE3 in the MA condition and type 316 stainless steel tubing tested at 700°C. The curve represents the average trend for nine heats of tubing evaluated by the National Research Institute for Metals (NRIM) in Japan.[9] Superimposed in the figure are the data produced on the two Eddystone heats. The archive heat ES1 is slightly below the average material, while the replacement heat ES2, of Japanese origin, is above average, partly because of a high residual element content. The CE3 alloy has twice the strength

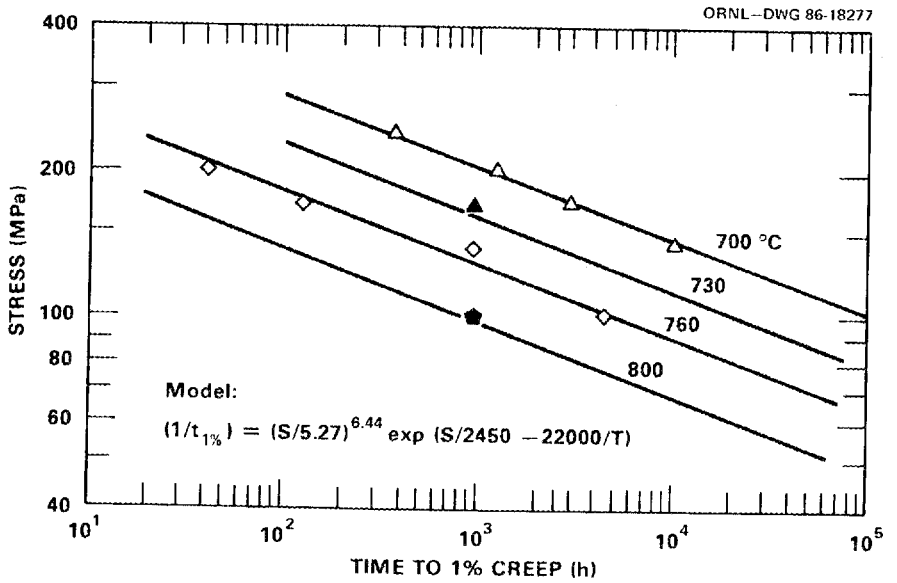

Fig. 13. Log stress vs log time to 1% creep for alloy CE3.

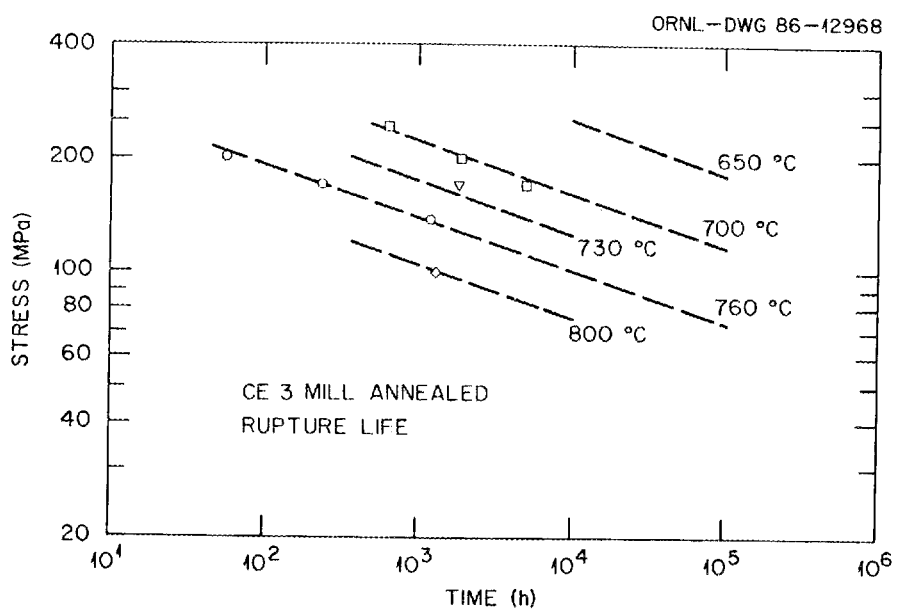

Fig. 14. Log stress vs log time to rupture for alloy CE3.

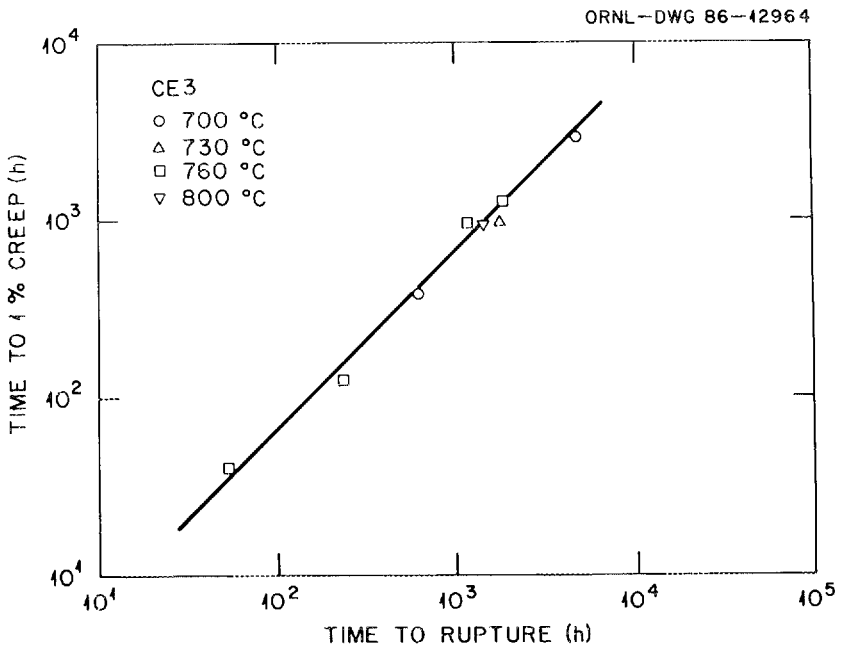

Fig. 15. Log time to 1% creep vs log time to rupture.

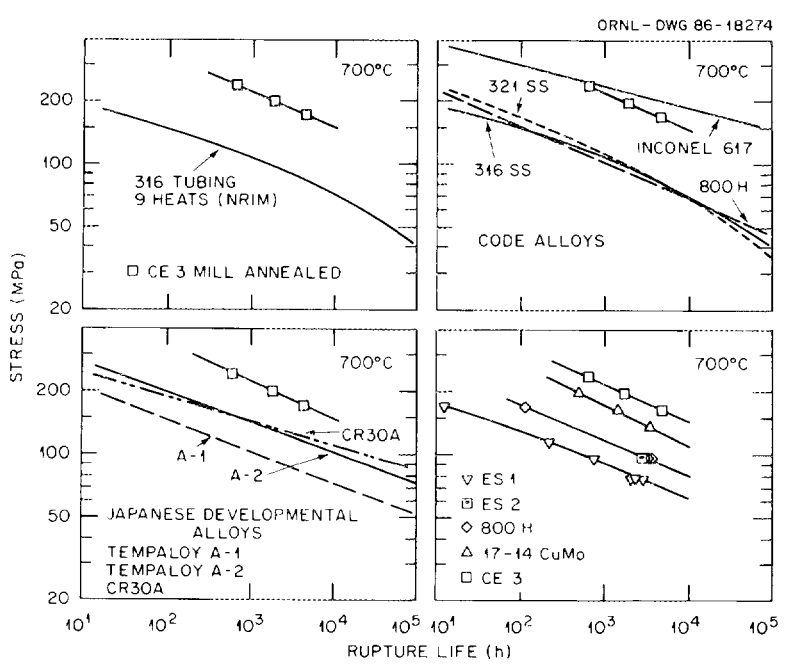

Fig. 16. Comparison of the creep rupture data for alloy CE3 with (*a*) type 316 tubing, (*b*) ASME Code alloys, (*c*) Japanese developmental alloys, and (*d*) reference alloys.

of these steels. In Fig. 16, the data for CE3 are compared with those of four alloys currently in ASME Code Sect. I – types 316 and 321 stainless steels, alloy 800H, and the nickel-base alloy 617. Relative to the iron-base alloys, the CE3 alloy has excellent strength and even approaches the strength of alloy 617. In Fig. 16, the average trends for several commercial Japanese alloys that have been developed for components in advanced steam systems are compared. These include Tempaloy A-1, which is a niobium-modified type 304 stainless steel; Tempaloy A-2, which is a niobium-titanium-modified type 316 stainless steel; and CR30A, which is a high-nickel high-chromium alloy intended as a superheater/reheater tubing material. See Table 7 for typical compositions. The strength of the CE3 alloy exceeds that of each Japanese alloy. It is pointed out, however, that there is significant heat-to-heat variation in these alloys and that some of the strongest heats in the Tempaloy A-2 and CR30A grades may match the strength of the CE3 alloy. In Fig. 15, the CE alloys are compared with the data produced on reference alloys – ES1, ES2, 17-14CuMo, and alloy 800. Comparison of the data on the reference alloys with the curves in Figs. 15 and 16 indicates that the reference alloys typify the trends reported in the literature. On the basis of this observation, the testing effort on ES1, ES2, and alloy 800 was diminished. Work on 17-14CuMo steel was continued because of the paucity of data.

LOW-STRESS CREEP TESTING

It appears that the lean stainless steel alloys (CE series) derive their strengths from various precipitate effects on dislocation structure and that stress and initial strain influence the formation of the precipitate microstructure in the early stages of the test which, in turn, produces the strength observed in the steady-state-creep regime. Because strain- and time-induced coarsening of the precipitates would eventually result in the loss of creep strength, better understanding of the nature of the strengthening and examination of the factors that alter the microstructure during the creep life are critical. The investigation of the issue includes relaxation testing at Cornell and a number of variable-stress, variable-temperature tests at ORNL. The tests are largely exploratory in nature and ongoing currently, so that only a few trends are discussed here.

Table 7. Typical chemical compositions of alloys for commercial superheater/reheater alloys (wt %)

Alloy	C	Si	Mn	Ni	Cr	Mo	Nb	Al	Ti	Fe	Other
Type 304H	0.06	0.63	1.61	8.75	18.22					Bal	
Type 316H	0.06	0.65	1.63	11.75	16.36	2.24				Bal	
Type 321H	0.06	0.44	1.54	10.72	17.47				0.39	Bal	
Type 347H	0.07	0.61	1.64	11.99	18.03		0.69			Bal	
Type 310S	0.06	0.68	1.67	20.84	24.40					Bal	
Type 314	0.10	2.33	1.52	19.58	24.27					Bal	
17-14CuMo	0.12	0.56	0.77	14.46	15.44	2.42	0.43		0.23	Bal	2.97Cu
Alloy 800H	0.07	0.57	0.90	31.91	21.16			0.49	0.50	Bal	
Alloy 807	0.09	0.69	0.93	39.13	21.06		1.19	0.27	0.48	Bal	8.12Co-4.6V
Alloy 617	0.06	0.16	0.03	Bal	22.92	9.20		0.85	0.48	0.52	11.55Co
Alloy 671	0.06	0.10	0.01	Bal	49.01				0.25		
Alloy 690	0.01	0.21	0.35	Bal	29.43					10.51	
Tempaloy F-9[a]	0.06	0.41	0.61		9.26	1.08	0.23			Bal	0.21V
Tempaloy A-1[a]	0.09	0.49	1.58	10.77	17.97		0.15		0.07	Bal	
Tempaloy A-2[a]	0.09	0.50	1.50	14.05	18.12	1.57	0.23		0.16	Bal	0.003B
Tempaloy CR30A[a]	0.06	0.27	0.20	50.99	30.52	2.11		0.14	0.18	Bal	0.05Zr
NAC Cr35A	0.07	0.07	0.01	46.15	35.04		0.52			Bal	

[a]Tempaloy is a registered trademark of the Nippon Kokan Steel Company.

Two tests were performed on the CE1 alloy at 700°C. In the first, the stress was held at 100 MPa for a time sufficient to reduce the rate of change of creep rate ($\dot{e}$) to a "minimum." This occurred at ~600 h and 0.15% creep, as indicated in Figs. 17 and 18. Figure 17 is a plot of creep strain vs time, while Fig. 18 is a plot of log $\dot{e}$ vs log e and reveals the rapid decrease in $\dot{e}$ that occurs in the first 0.1% creep. After $\dot{e}$ stabilized, excursions in stress were performed, both upward and downward, over a period of ~5000 h. The $\dot{e}$ both before and after the excursions was examined to evaluate the stress dependence of $\dot{e}$ at constant structure. The inserts in Fig. 17 indicate how the creep rate changed after two of these transients. In both cases, an almost constant $\dot{e}$ was observed, indicating little or no immediate change in microstructure. A plot of log $\dot{e}$ against log stress produced in this manner is provided in Fig. 19. Here the stress dependency of $\dot{e}$ appears to follow a power law of the form

$$\dot{e} = aS^n \ , \tag{2}$$

where n is near 11. In a second test on alloy CE1, the specimen was loaded to 170 MPa and the stress was reduced incrementally to maintain constant strain within 20 μe. This technique produced a relaxation-type response in which the $\dot{e}$ could be determined for reducing stresses at near-constant total strain. The relaxation period was 1000 h; it produced a final stress that was below the 100 MPa of the previous test. The relaxation test was then repeated (run 2). The $\dot{e}$ data produced in the relaxation test are included in Fig. 18 and show good agreement with the $\dot{e}$ data accumulated in stress-change tests. With the accumulation of time and strain approaching 1%, however, there was a gradual change in $\dot{e}$ that decreased n to ~6. This shift is shown in Fig. 19.

Recovery-creep experiments were also performed on alloys CE1 and CE3. Here, the period of time necessary to exhaust the back-stress effect was measured for partial load reductions, and the magnitude of the recovery creep at zero stress was determined for a 24-h recovery period. At 700°C, most of the back-stress effects were exhausted in ~24 h, and the maximum recovery strain was ~20% of the prior elastic strain. The trend is illustrated in Fig. 20, which plots the recovery strain in 24 h

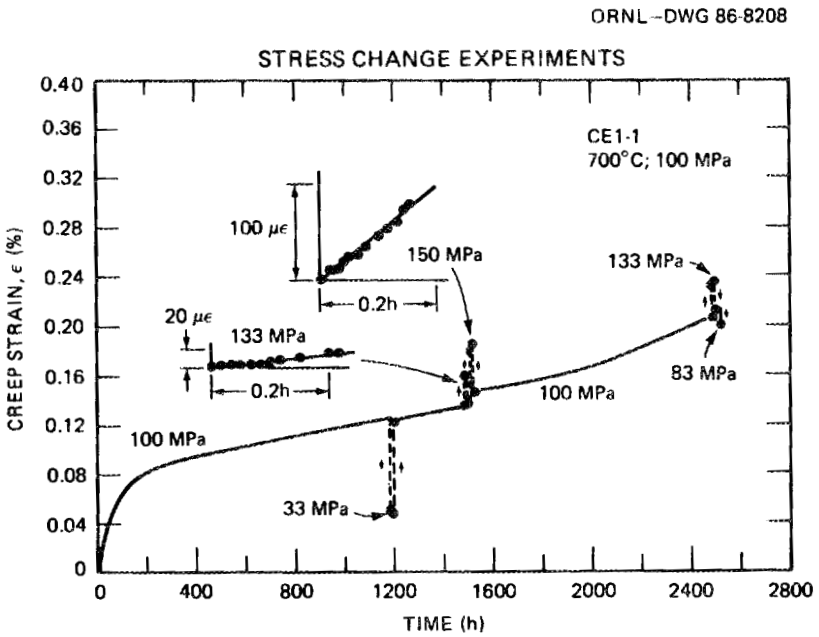

Fig. 17. Creep strain vs time for alloy CE1 at 700° C and 100 MPa. Inserts show the response after stress changes.

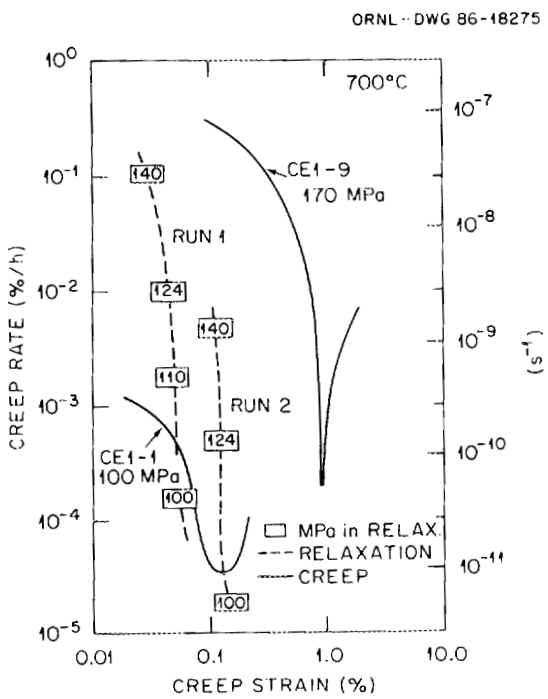

Fig. 18. Log creep rate vs log creep strain for alloy CE1. Data from constantload and relaxation tests are included.

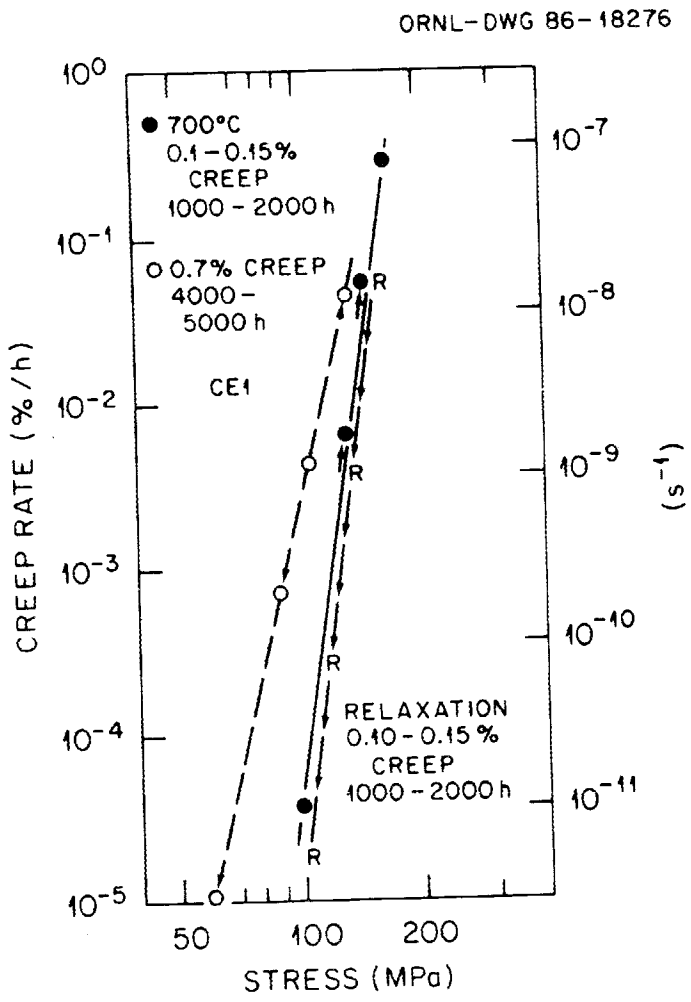

Fig. 19. Log creep rate vs log stress. Data produced from stress change tests at 700°C.

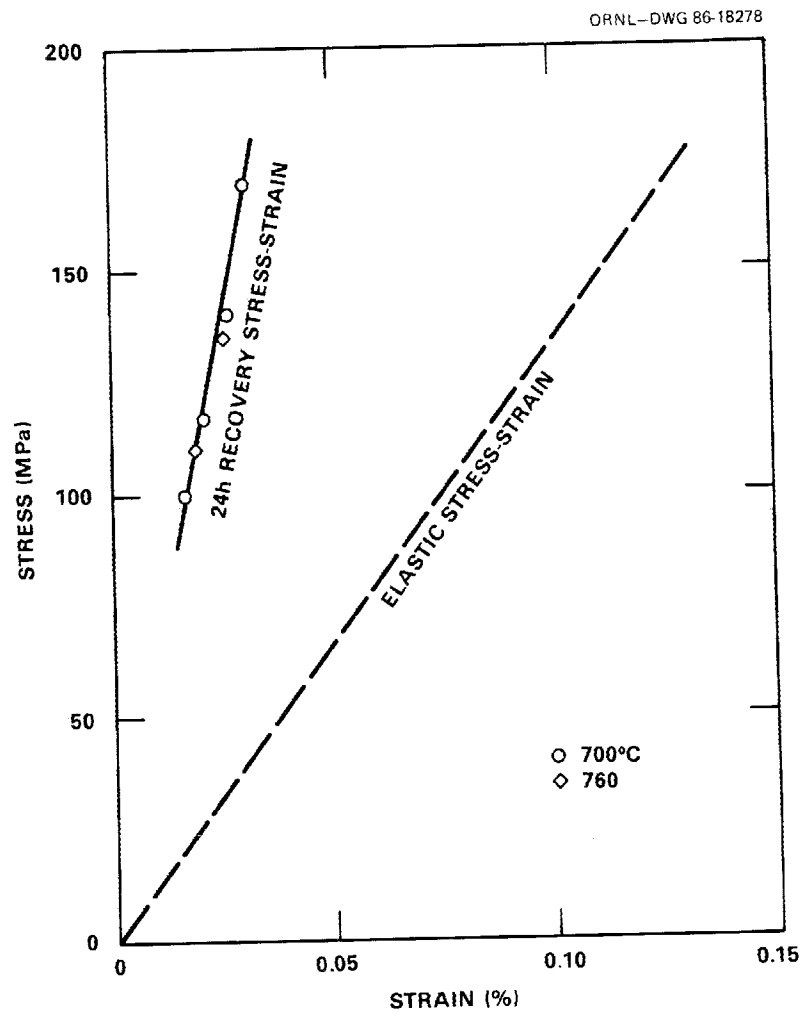

Fig. 20. Creep recovery strain in 24 h vs stress change for alloys CE1 and CE3 at 700°C.

against the stress change. The behavior is indicative of either a low back-stress effect relative to other austenitic alloys studied in this manner[10] or a low rate of recovery creep. Upon reloading, the short-time transient was exhausted in a few hours, and, by the time the creep strain returned to the same value as before the stress reduction, the creep rate diminished to the original value. This trend suggested that it was a low back stress rather than low recovery creep rate that was responsible for small recovery strains.

MICROSTRUCTURAL EXAMINATION

Microstructural examinations consisted of both optical microscopy and analytical electron microscopy. To complement the studies on the precipitation component of the microstructure, bulk extraction of precipitates was also performed to determine the weight fraction. In addition to examination of as-received or mechanically tested specimens, specimens of the various developmental and reference alloys were examined after completion of aging and/or annealing experiments to gain additional insight into precipitation mechanisms of the advanced austenitics or to better compare those austenitics with the reference alloys.

OPTICAL MICROSCOPY

Optical microscopy was used to help evaluate the annealing behavior of several of the CE series alloys. Figure 21 shows the effect of varying reannealing conditions on the mill-annealed CE0 alloy. Annealing for 1/2 h at 1115°C only partially recrystallized the material and appeared to leave the stringers of precipitates that were present in the mill-annealed material undissolved [Fig. 21(*a*) and (*b*)]. Annealing for 1 h at 1200°C definitely recrystallized the material and appeared to dissolve some of the finer background precipitation [Fig. 21(*c*)]. Annealing for 1 h at 1275°C produced a larger uniform grain size than did annealing at 1200°C, and it either dissolved or coarsened the finer precipitates in the matrix. The largest precipitates remained relatively unchanged; they are most likely primary inclusions of Ti/Nb carbo-nitrides.

Figure 22 compares CE1 and CE3 alloys after reannealing for 1 h at 1250°C, after they have been reduced to 30-mil-thick sheet from the

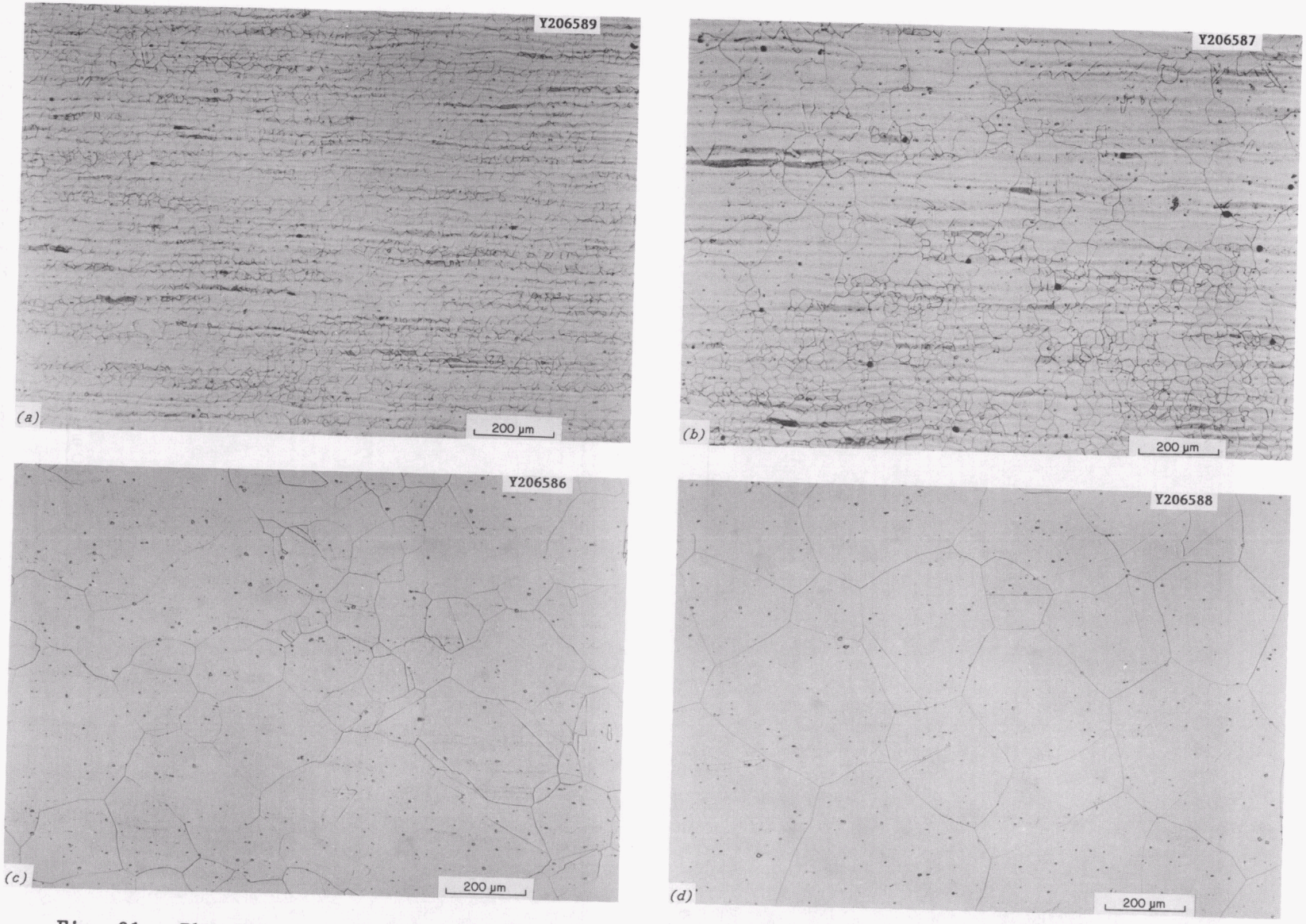

Fig. 21. Photomicrographs showing the effects of annealing on grain microstructure in the CE0 alloy. (*a*) Mill-annealed; (*b*) 1/2 h at 1115°C; (*c*) 1 h at 1200°C; (*d*) 1 h at 1275°C.

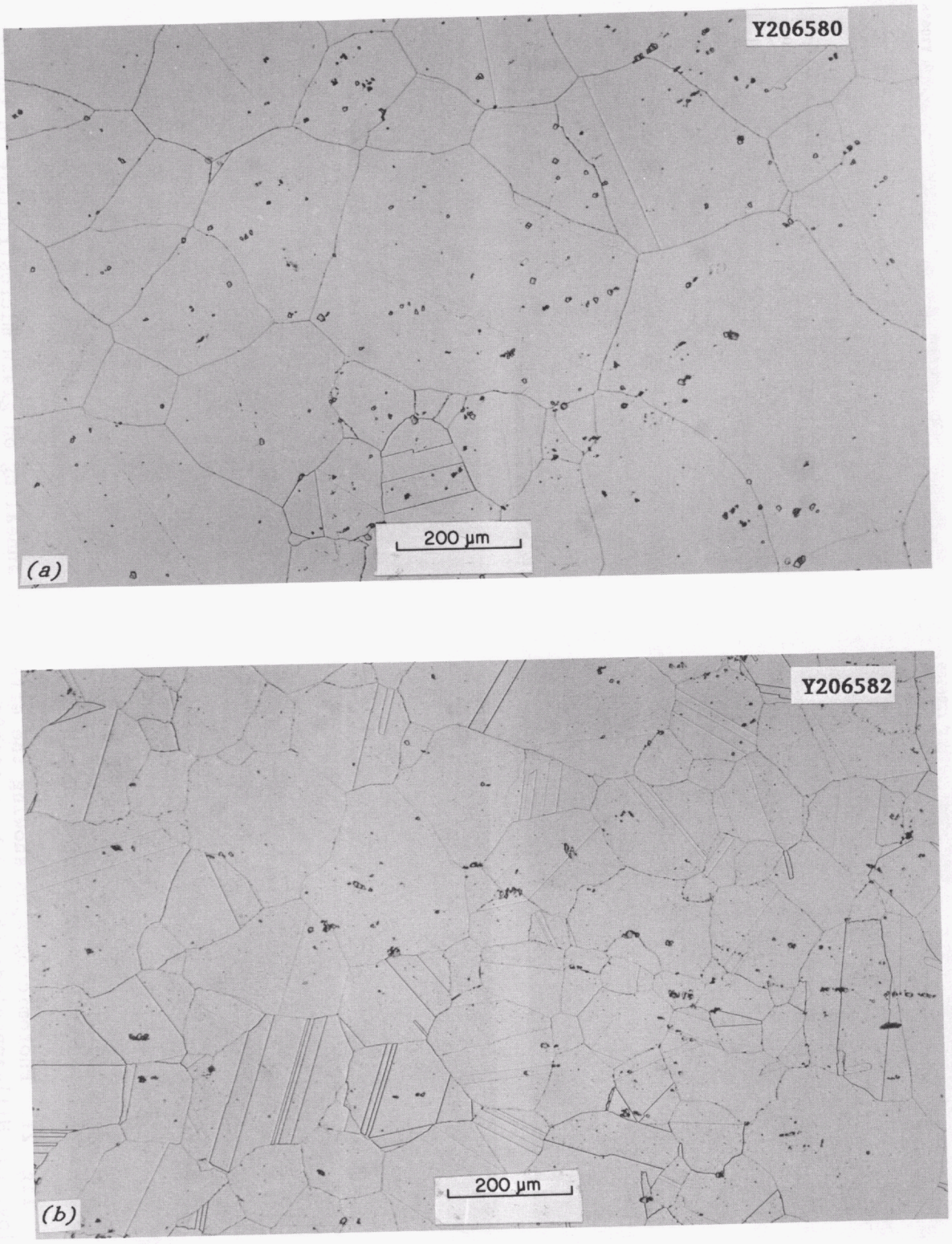

Fig. 22. Photomicrographs of (*a*) CE1 and (*b*) CE3 after annealing for 1 h at 1250°C.

as-received, mill-annealed condition. CE3 appears similar to CE0 in Fig. 21(*c*) in terms of grain size, but with less finer matrix precipitation. By contrast, CE1 has a slightly finer grain size but more fine matrix precipitation, and it definitely has fine precipitates along the grain boundaries. The primary inclusions are clustered in CE1, whereas they are fairly uniformly distributed in the other alloys.

Optical microscopy was also used to examine the general features of the creep failures. These features were invariant in the CE series of alloys. All failures occurred by plastic instability that was manifested by the development of a neck in the gage of the specimen, the growth of plasticity-induced cavities at inclusions, and transgranular rupture produced by the linking of the cavities. A typical failure cross section is illustrated by the photomicrographs in Fig. 23 obtained from alloy CE3 after failure in 4940 h at 700°C. Globular precipitates were present on the boundaries of greatly elongated grains, and only a few large precipitates were observed within the grains at magnifications up to 1000 diameters. Grain boundary cracking was found near the surface of specimens that were tested for long times, as shown in Fig. 24 for alloy CE2 that failed after 2365 h with 41.5% reduction of area. Here the oxide penetrated along grain boundaries both perpendicular and parallel to the applied stress. Heavy oxidation was present also in the grains near the surface. The threaded ends also exhibited heavy scale and near-surface oxidation.

Chemical etchants revealed no trace of sigma or other intermetallic phases on the grain boundaries of the CE series of alloys.

Because creep rupture failures were not produced in the AMAX series, no optical metallography can be reported at this time.

EXTRACTION OF BULK PRECIPITATES

Precipitates were extracted from bulk specimens by electrolytic etching using a 10% HCl in methanol solution, and the residues were weighed to determine the total weight fraction of precipitates present. These measurements were made on various alloys after annealing or aging treatments, or after creep testing. Results are given in Tables 8 and 9.

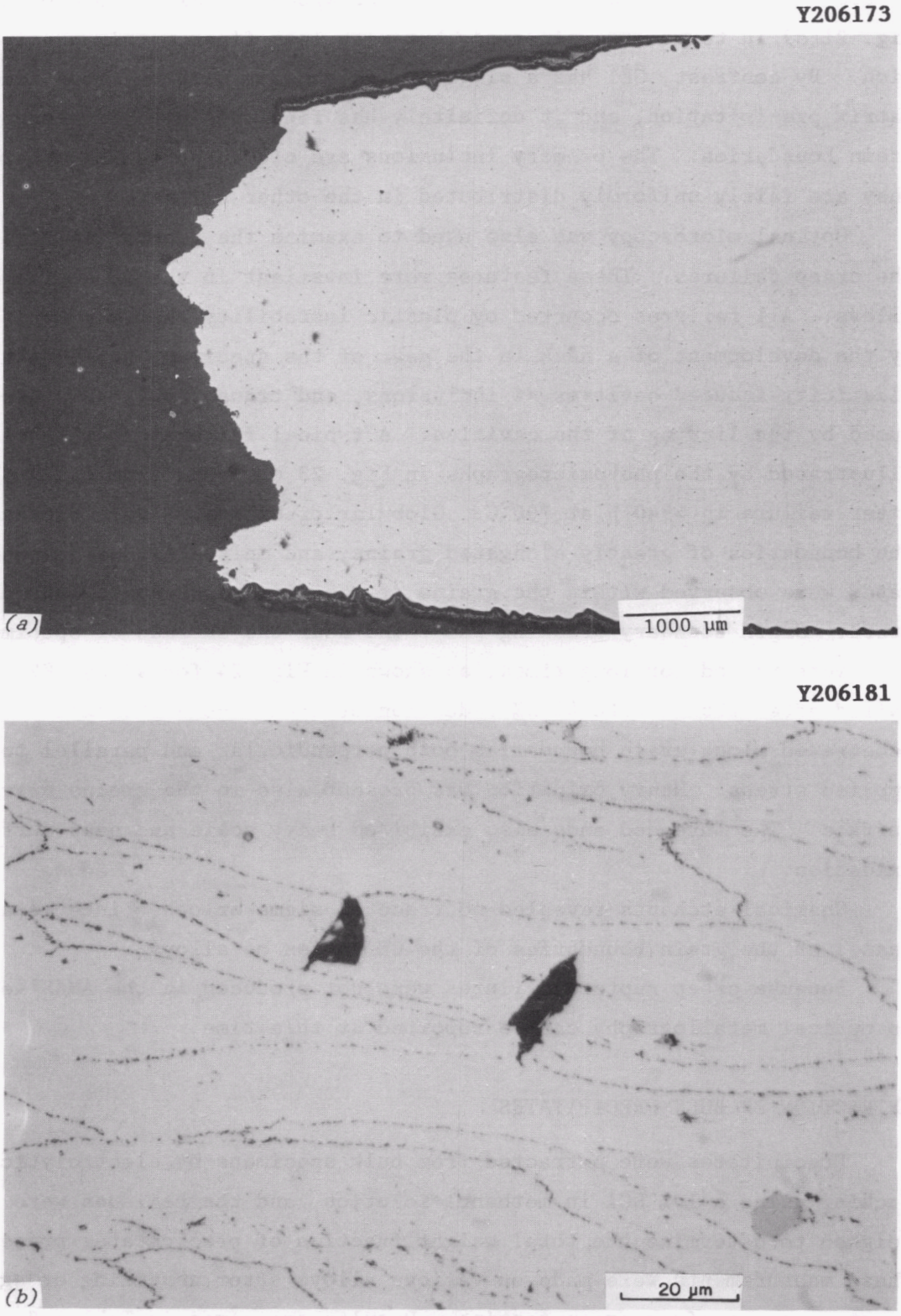

Fig. 23. Photomicrographs showing the cross section of a specimen of alloy CE3 that failed in 4940 h at 700°C. (*a*) Necked region. (*b*) Plasticity-induced transgranular cracks.

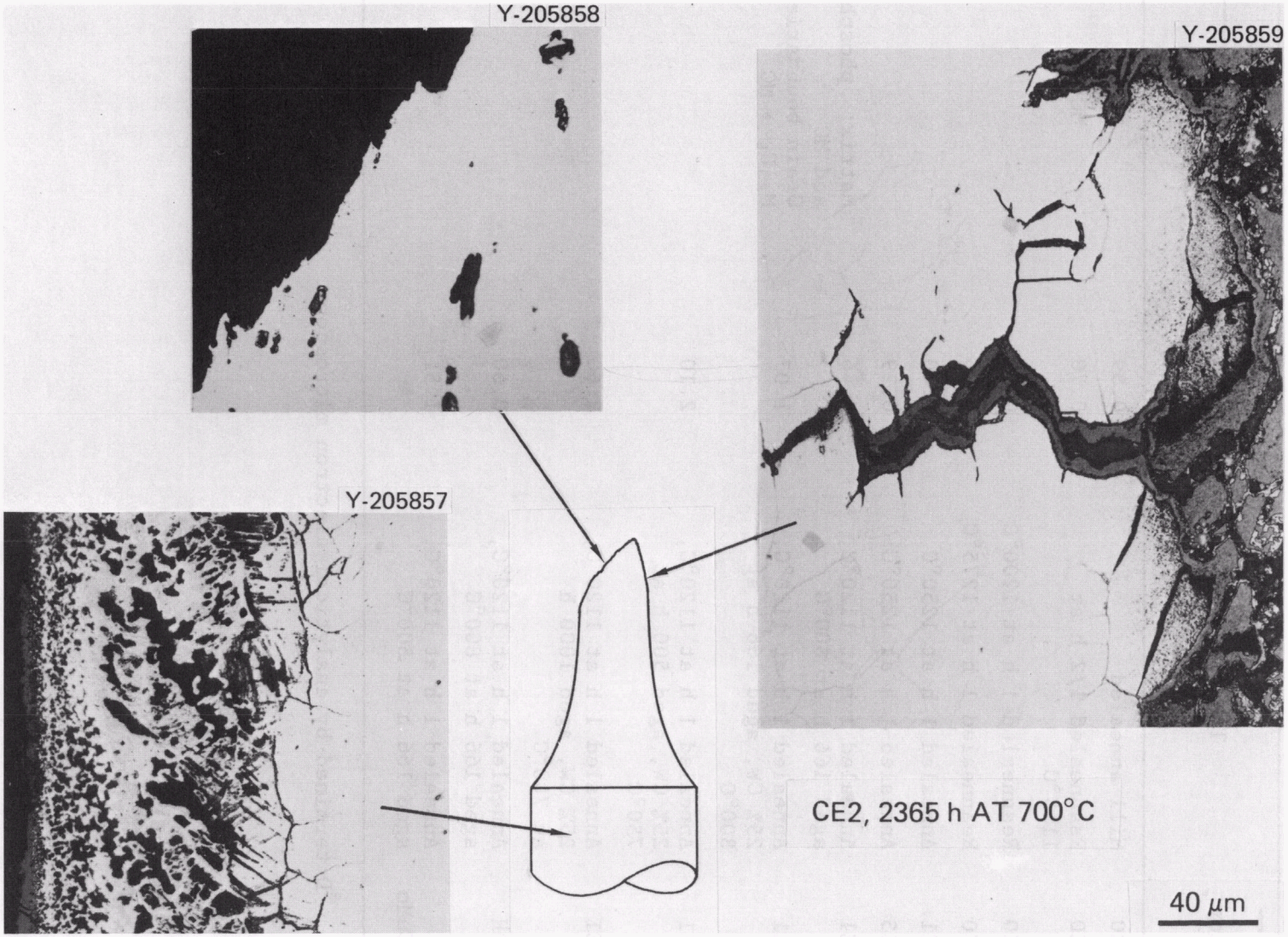

Fig. 24. Photomicrographs of a typical near-surface region of the CE series of alloys. Internal oxidation is severe, and penetration is deep along grain boundaries.

Table 8. Precipitation analysis in annealed and/or aged alloys

Alloy	Treatment	Precipitate analysis	
		Extracted amount (wt %)	Phases[a]
CE0	Mill annealed	0.39	MC
CE0	Reannealed 1/2 h at 1115°C	0.70	MC
CE0	Reannealed 1 h at 1200°C	0.27	
CE0	Reannealed 1 h at 1275°C	0.56	
CE1	Annealed 1 h at 1250°C	0.40	
CE3	Annealed 1 h at 1250°C	0.29	
CE1	Annealed 1 h at 1120°C, aged 166 h at 800°C	0.46	Matrix: phosphides and MC Grain boundaries: $M_{23}C_6$ + MC
CE1	Annealed 1 h at 1120°C, 25% CW, aged 166 h at 800°C	1.07	
CE1	Annealed 1 h at 1120°C, 25% CW, aged 500 h at 750°C	2.10	
CE1	Annealed 1 h at 1120°C, 25% CW, aged 1000 h at 700°C	2.60	
800H	Annealed 1 h at 1120°C, aged 166 h at 800°C	0.60	
17-14CuMo	Annealed 1 h at 1120°C, aged 166 h at 800°C	1.51	

[a]Determined by analytical electron microscopy.

Table 9. Precipitation analysis in creep-tested alloys

Alloy	Treatment and condition	Precipitate analysis	
		Extracted amount (wt %)	Phases[a]
ES 316	Mill annealed, tested at 700°C and 170 MPa, rupture in 12 h	Gage, 0.57	Matrix and grain boundaries: $M_{23}C_6$
800H	Mill annealed, tested at 700°C and 170 MPa, rupture in 120 h	Gage, 1.36	Matrix: $M_{23}C_6$ + MC Grain boundaries: $M_{23}C_6$
17-14CuMo	Mill annealed, tested at 700°C and 140 MPa, rupture in 3446 h	Gage, 2.70 Shoulder, 1.80	Matrix: MC Grain boundaries: Laves
CE0-2	Solution annealed 1/2 h at 1115°C, tested at 700°C and 170 MPa, no rupture after 533 h	Gage, 1.82	Matrix: MC + phosphides Grain boundaries: $M_{23}C_6$ + M_6C + Laves
		Shoulder, 1.53	Matrix: MC + phosphides Grain boundaries: $M_{23}C_6$ + M_6C
CE0-3	Mill annealed, tested at 700°C and 170 MPa, no rupture after 692 h	Gage, 1.61	Matrix: MC + phosphides Grain boundaries: $M_{23}C_6$ + MC + M_6C
		Shoulder, 1.22	Matrix: phosphides + MC Grain boundaries: M_{23} + MC + phosphide + M_6C + Laves
CE2-15	Mill annealed, tested at 700°C and 170 MPa, rupture in 2365 h	Gage, 0.88	Not determined
		Shoulder, 2.11	Not determined
CE3-1	Mill annealed, tested at 700°C and 170 MPa, rupture in 4960 h	Gage, 1.34	Matrix: phosphides + MC Grain boundaries: $M_{23}C_6$ + M_6C + MC + Laves + Cu
		Shoulder	Not determined
CE3-6	Mill annealed, tested at 760°C and 200 MPa, rupture in 53.8 h	Gage, 1.40	Not determined
CE3-2	Mill annealed + 24 h at 850°C, tested at 700°C and 170 MPa, rupture in 3795 h	Gage, 1.45 Shoulder, 4.31	Not determined Not determined

[a]Determined by analytical electron microscopy.

The reannealing study of CE0 showed that the maximum precipitation developed at 1115°C (Table 8). Precipitation was lower in the MA material and lowest in the material reannealed at 1200°C. The amount of precipitate is slightly higher after reannealing at 1275°C, but the reason for that change is not known. The CE1 and CE3 alloys also had a low amount of residual precipitation when annealed after processing to thin sheet, with CE3 having slightly less.

Isothermal, stress-free aging of solution annealed (SA) CE1 for 166 h at 800°C produced a small amount of additional precipitation (Table 8). Much more precipitation is produced in CE1 when it is similarly aged in the 25% cold worked (CW) condition. Even more precipitation occurs in 25% CW CE1 after longer times at lower temperatures (700 and 750°C). By comparison to the SA CE1, the 800H alloy has slightly more and the 17-14CuMo has much more precipitation when aged in the SA condition at 800°C for 166 h.

A few of the many samples that were creep tested were also examined to analyze precipitation and microstructure. However, the comparisons are not systematic and are incomplete because the specimens available first were those that had failed after shorter times (better behaving alloys and those with thermal-mechanical pretreatments are lasting for very long times) or had come from discontinued tests. The bulk extraction results are presented in Table 9.

Of the specimens tested in the mill-annealed condition at 700°C and 170 MPa, the Eddystone 316 showed the least precipitation in the gage region, whereas the 17-14 CuMo showed the most (Table 9). The amounts of precipitation were intermediate and similar at about 1.5 wt % in alloys 800H, CE0, and CE3, with CE2 having less. The low- or no-stress shoulder regions of these same specimens showed less precipitation for the 17-14CuMo and CE3 alloys, slightly less for the CE0 alloy, but more for the CE2 alloy. CE0 was similarly creep tested after reannealing the mill-annealed material for 1/2 h at 1115°C, and the amount of precipitation increased slightly in both the gage and the shoulder relative to the mill-annealed material. CE3 was similarly creep tested after aging the mill-annealed material for 24 h at 850°C. Precipitation also increased in the

gage relative to unaged material, and it greatly increased in the shoulder. Finally, mill-annealed CE3 showed a similar amount of precipitation when tested for a short time (55.8 as compared to 4940 h) at higher stress and temperature (200 MPa, 760°C).

ANALYTICAL ELECTRON MICROSCOPY

Analytical electron microscopy (AEM) was used to examine the precipitate and dislocation components of the microstructure in thin foils, and to identify phases and measure their compositions and relative fractions on extraction replicas. Phase indentification analyses for various samples are included in Tables 8 and 9. This facet of the overall experimental effort aimed at evaluating the advanced austenitics is the least complete because the AEM observations are laborious and because AEM samples are the last in the chain of samples that must be prepared from a specimen after heat treating or mechanical testing. Examination of alloys CE0 through CE3 is under way, whereas examination of the AMAX series has not yet been started.

Transmission electron microscopy (TEM) of CE0 in the MA condition, as well as after reannealing for 1/2 h at 1115°C and for 1 h at 1200°C, is shown in Fig. 25. It can be seen that the MA material contains a cellular array of subgrain boundaries with a loose dislocation network within the cells. By contrast the material reannealed at 1115°C has only a few dislocations and recovery of the subgrain structure, and the material reannealed at 1200°C is nearly dislocation free. The material reannealed at 1115°C also has the most MC, distributed both as coarse particles within the grains and finer particles along dislocation lines, consistent with measured precipitate weight fractions (see Table 8). The material reannealed at 1200°C has no fine MC and few coarser particles, at least on the scale of TEM.

The aging response for CE1 was observed after reannealing for 1 h at 1120°C. Aging for 166 h at 800°C produced an abundant mixture of coarse and very fine dense phosphide needles and some coarse MC particles in the matrix, and dispersion of fine MC and coarse $M_{23}C_6$ particles along the grain boundaries (Fig. 26). Aging for 1000 h at 700°C produced somewhat similar precipitate distributions along grain boundaries, but far less matrix precipitation (Fig. 27). In contrast to the dense array of fine

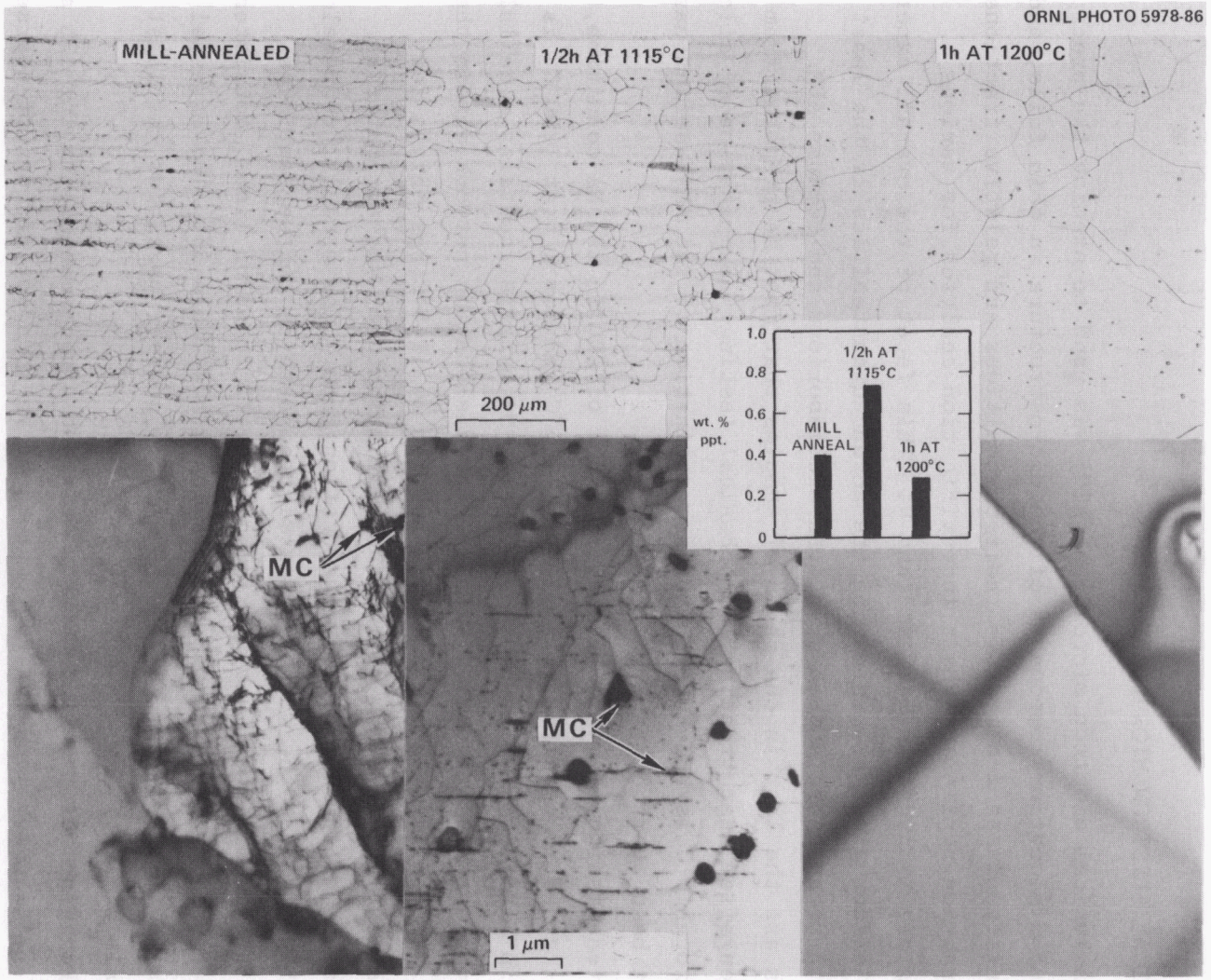

Fig. 25. Microstructural comparison of CEO in the as-received mill-annealed condition as well as after reannealing for 1/2 h at 1115°C and 1 h at 1200°C, at low magnification via optical metallography (top micrographs) and high magnification via transmission electron microscopy (bottom micrographs). The weight fraction of precipitate measured in each of these samples is given in the inset.

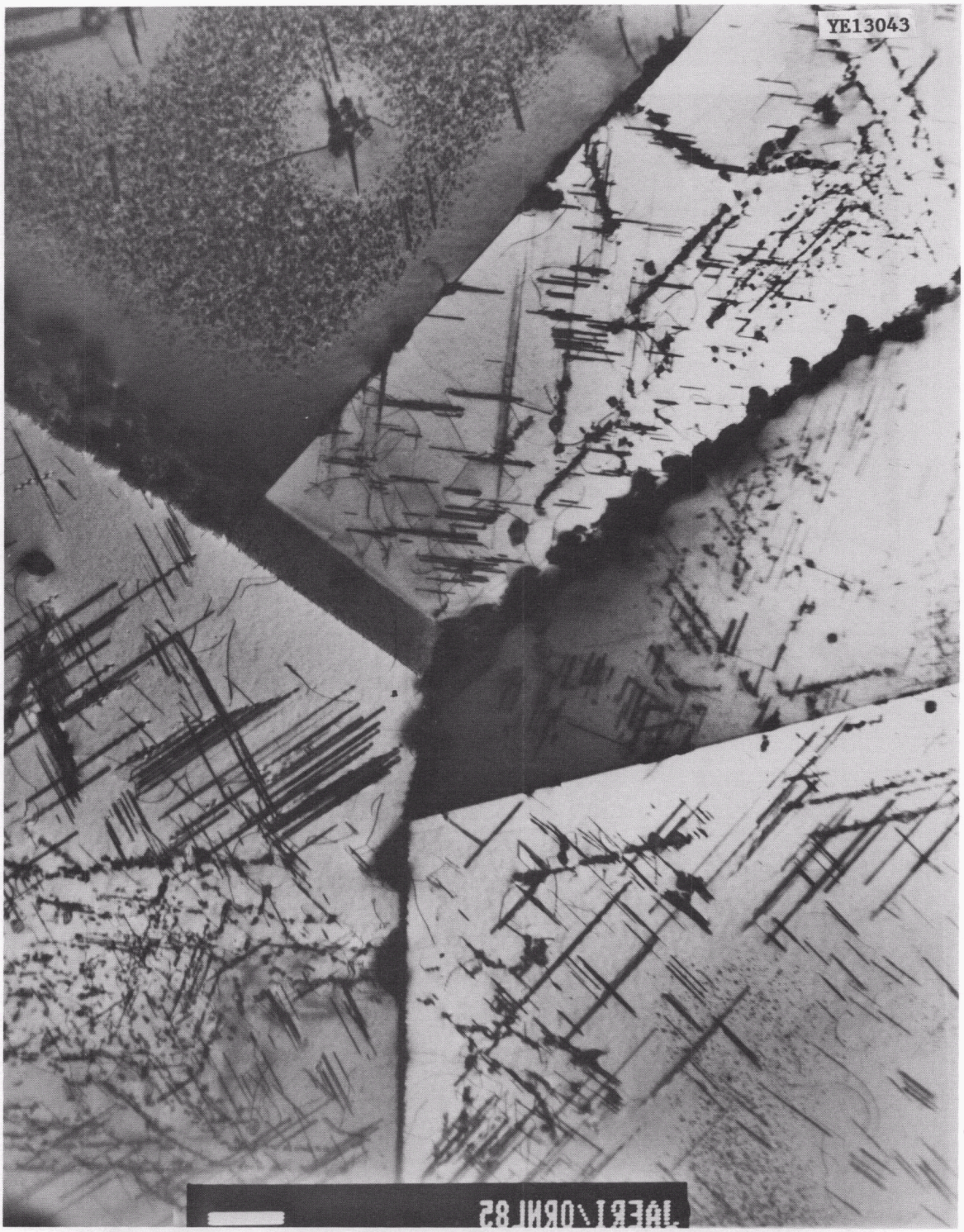

Fig. 26. Transmission electron micrograph of alloy CE1 showing distribution of phosphide needles, coarse $M_{23}C_6$ precipitates on the grain boundary, and fine MC precipitates.

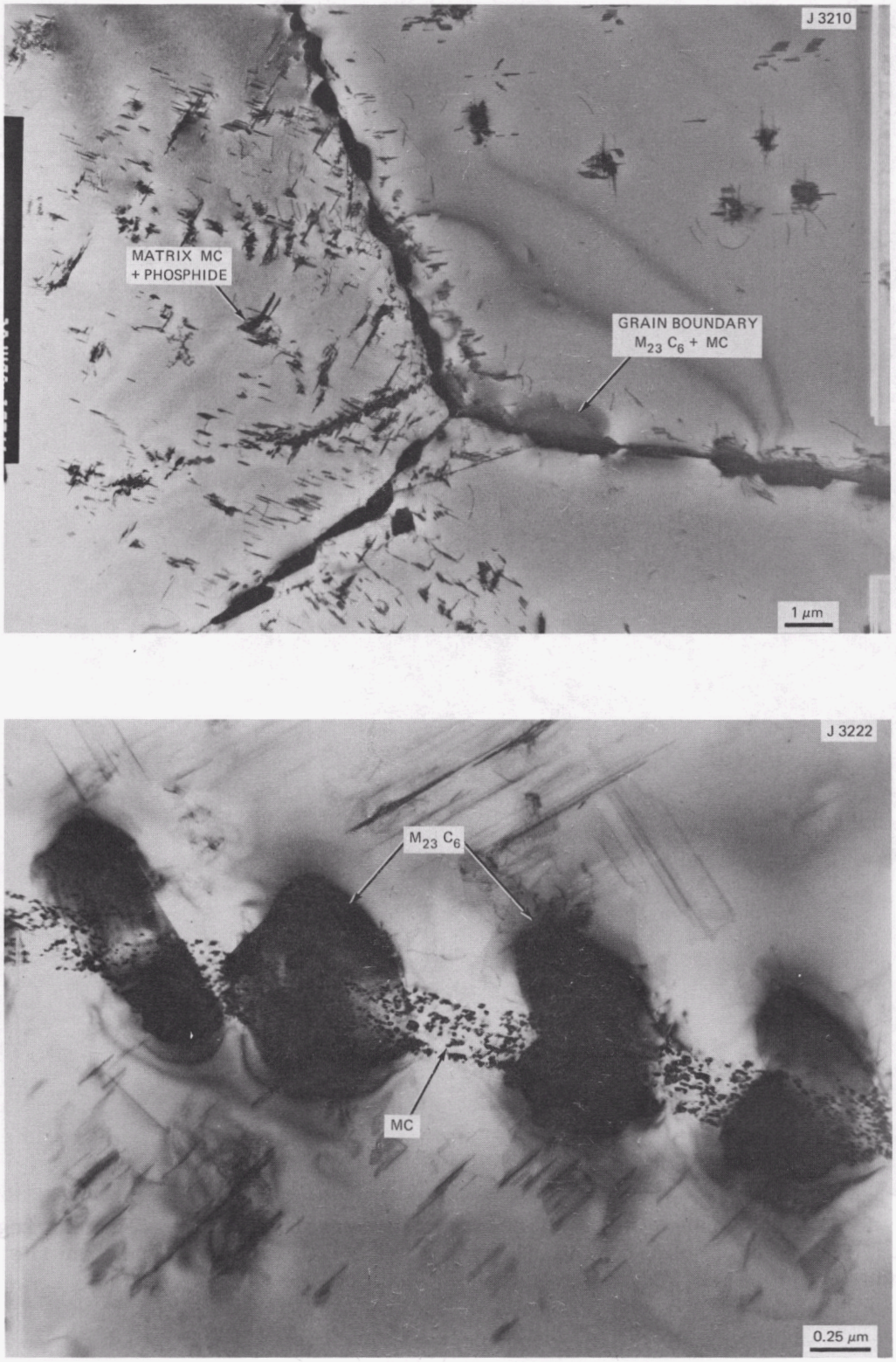

Fig. 27. Microstructure via TEM of CE1 reannealed for 1 h at 1120°C and then aged 1000 h at 700°C, with (*a*) matrix at lower magnification and (*b*) grain boundary at higher magnification.

phosphide needles present at 800°C, needles appear clustered around coarser MC particles or along dislocation lines at 700°C, suggesting that nucleation is more difficult. The microstructure of solution-annealed 316 (DO-heat) is shown after aging at 800°C for 166 h in Fig. 28. It has only sparse precipitation of coarse $M_{23}C_6$ and Laves particles in the matrix at grain boudaries, with possibly some chi. One can therefore appreciate the uniqueness of the fine precipitation in CE1 by comparison, which was one of the objectives for designing the alloy.

The microstructures of several specimens, including CE0, CE3, ES 316, 800H, and 17-14CuMo, were examined after creep at 700°C. The ES 316 developed a dispersion of coarse grain boundary $M_{23}C_6$ precipitates after creep at 700°C and 170 MPa, but virtually no precipitation in the matrix, as shown in Fig. 29. The dislocation structure is a cellular array of dense network regions and completely recovered regions, consistent with the rapid failure of this specimen with little creep strength. Alloy 800H showed precipitation of elongated and aligned $M_{23}C_6$ particles along very straight grain boundaries, which may contribute to the change in failure mode from ductile-transgranular to brittle-intergranular relative to the ES 316 (see Fig. 30). The matrix contained fine precipitates of titanium-rich MC and coarser $M_{23}C_6$, and a looser, spacially more uniform dislocation structure relative to ES 316, suggesting that these precipitates provide the slightly better creep resistance seen in 800H. By contrast to either of these steels, the modified alloys, CE0 and CE3, showed unique matrix structures, fine MC, and needle-phosphide precipitates that appear to be pinning all of the loose network dislocations visible in the microstructure, as shown in Fig. 31 for CE3, consistent with dramatically improved creep resistance manifested by these alloys. The grain boundaries contain a saw-tooth array of coarse $M_{23}C_6$ particles with occasional M_6C, Laves, or MC forming adjacent to them. These grain boundary precipitates in CE3 may be responsible for transition back to an intragranular-ductile failure mode relative to intergranular-brittle behavior manifest in 800H and 17-14CuMo at 700°C and 170 MPa. All of the above samples were evaluated in the as-received mill-annealed condition.

Examination of several other CE0 TEM specimens illustrates the uniqueness and importance of the similar fine MC and phosphide needle

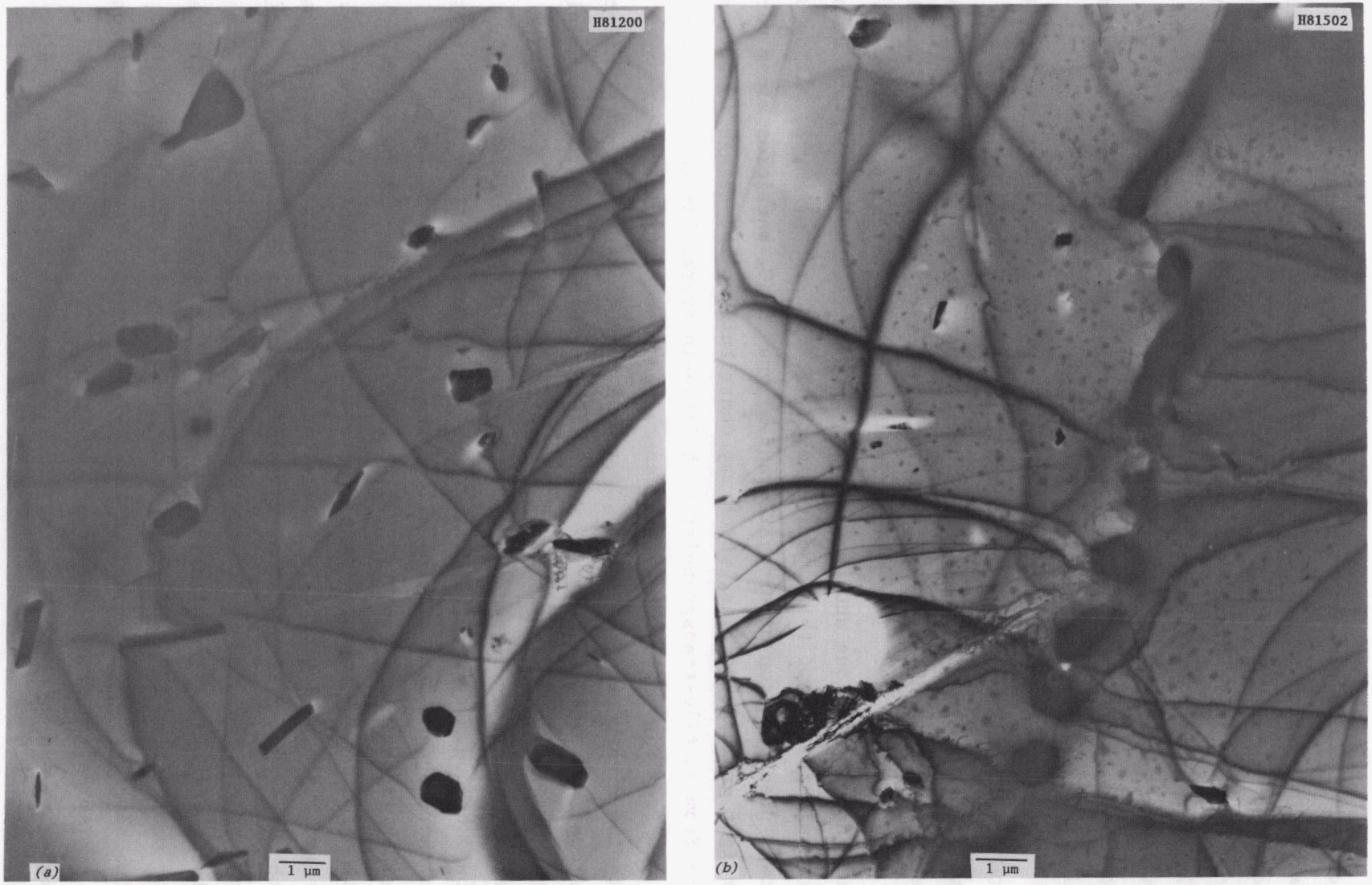

Fig. 28. Microstructure of (*a*) matrix $M_{23}C_6$ and Laves particles and (*b*) grain boundary $M_{23}C_6$ and Laves particles in solution-annealed DO-heat type 316 stainless steel aged for 166 h at 800°C.

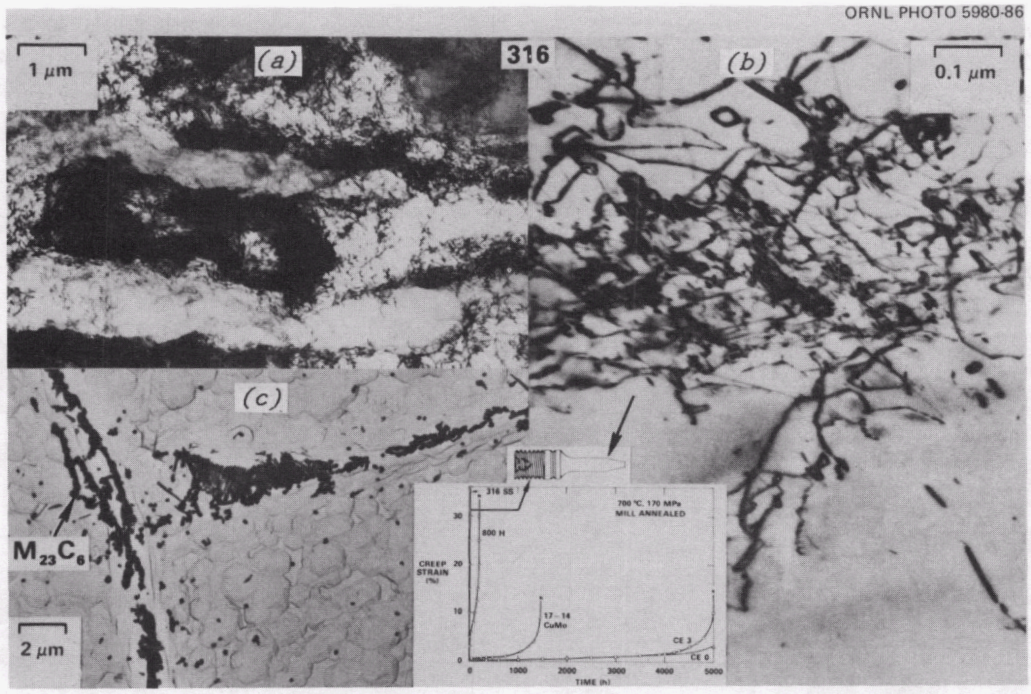

Fig. 29. Microstructures of the gage portion of ES 316 after creep testing at 700°C and 170 MPa, showing (*a*, *b*) the matrix dislocation structure in a thin foil at low and high magnifications, respectively, and (*b*) grain-boundary $M_{23}C_6$ precipitates on an extraction replica. The inset shows the creep curve for this specimen and the location on the sample from which the TEM specimen was cut.

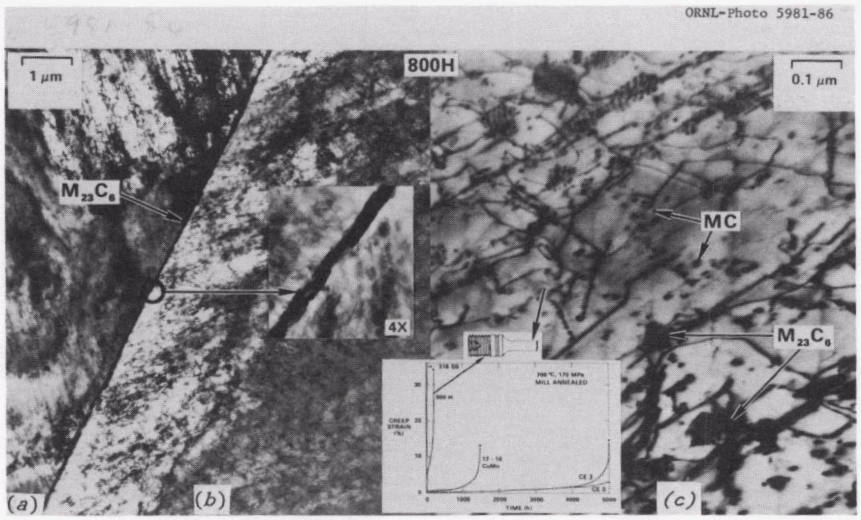

Fig. 30. Microstructure of the gage portion of 800H (mill-annealed) sample after creep testing at 700°C and 170 MPa showing (*a*) grain boundaries, with $M_{23}C_6$ precipitates, and (*b*) matrix, with fine MC and coarser $M_{23}C_6$ precipitates. The inset shows the creep curve for this specimen and the location on the sample from which the TEM specimen was cut.

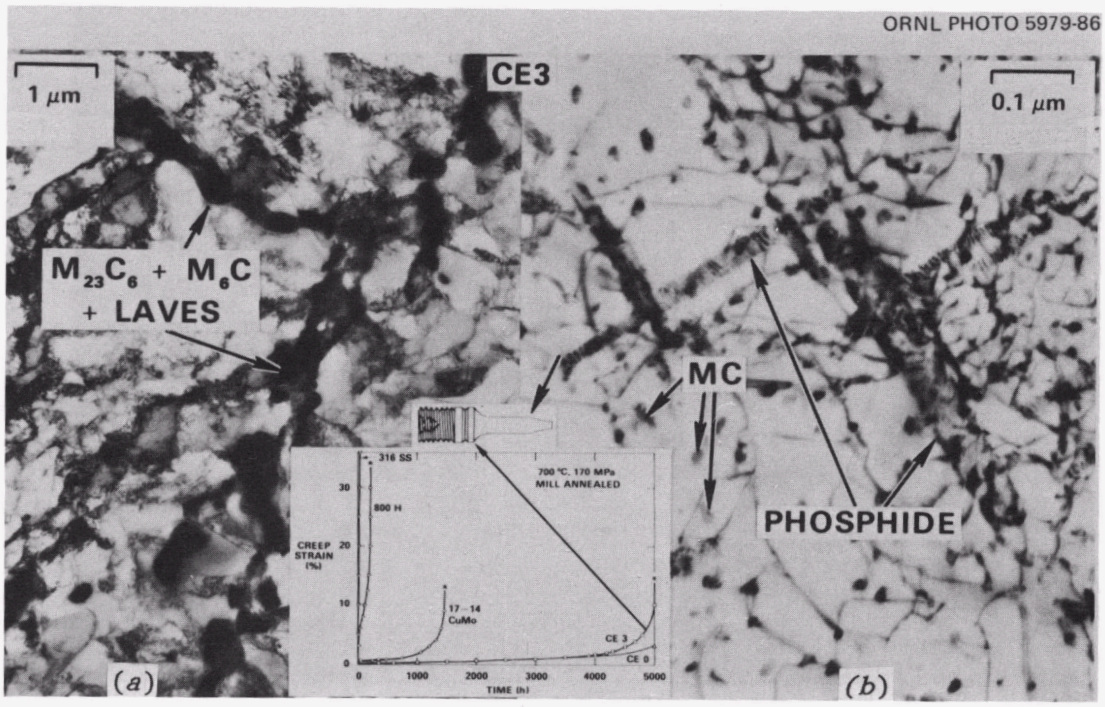

Fig. 31. Microstructure of the gage portion of mill-annealed CE3 sample after creep testing at 700°C and 170 MPa showing (*a*) grain boundaries with primarily $M_{23}C_6$ and some M_6C and Laves phase precipitates, and (*b*) matrix with fine MC and needle-phosphide precipitates. The inset shows the creep curve for this specimen and the location on the sample from which the TEM specimen was cut.

microstructures that develop in CE0 and CE3 during creep at 700°C. First, the mill-annealed structure of CE0 has none of the fine precipitates that are found during creep (Fig. 24). Second, the shoulder portion of the CE0 mill-annealed specimen (same time at temperature but with little or no stress) shows some of the fine MC and phosphide precipitation on dislocation subgrain boundaries in Fig. 32, but none of the abundant precipitation of these same phases that fills in these subgrains during creep. Finally, as is also shown in Fig. 32, reannealing at 1115°C causes coarse MC to form prior to creep testing (Fig. 24), which then interferes with the precipitation of fine particles as seen in mill-annealed CE0 by depleting important alloying elements from the supersaturated solid solution.

Compositional analysis of precipitate phase particles on carbon extraction replicas with quantitative X-ray energy dispersive spectroscopy (XEDS) is under way. The results are very preliminary and incomplete, but several important observations are worth making here. The fine matrix phases formed in alloys CE0 and CE3 during creep at 700°C are phosphides and MC. Occasional phosphide needles can be found in similarly creep tested 800H, but, as Fig. 33 shows, there are important differences in their compositions relative to those found in the advanced austenitics. The phosphide particles in CE3 more nearly resemble FeTi phosphides, with incorporation of V, Nb, and Mo but very little Cr and Ni. These compositional characteristics are probably important to the formation and stability of the phosphides found in the advanced austenitics. Figure 34 shows that there are also important compositional differences in the MC phase that forms during creep at 700°C in the 800H, 17-14CuMo, and CE3 alloys. The MC formed in CE3 has substantial enrichments of Ti, V, and Nb with less Cr and/or Si than the other two alloys; the Ti, Nb, and V were deliberately added to the advanced austenitic steels with the thought that they would interact in the formation of a complex MC phase. Finally, analysis of grain boundary phases, as typified by the example in Fig. 35 of SA CE1 aged for 166 h at 800°C, shows that the predominant coarse phase at the boundaries is Cr-rich $M_{23}C_6$, with, in this case, fine and coarse MC particles as well. The comparison of fine and coarse MC particles shows

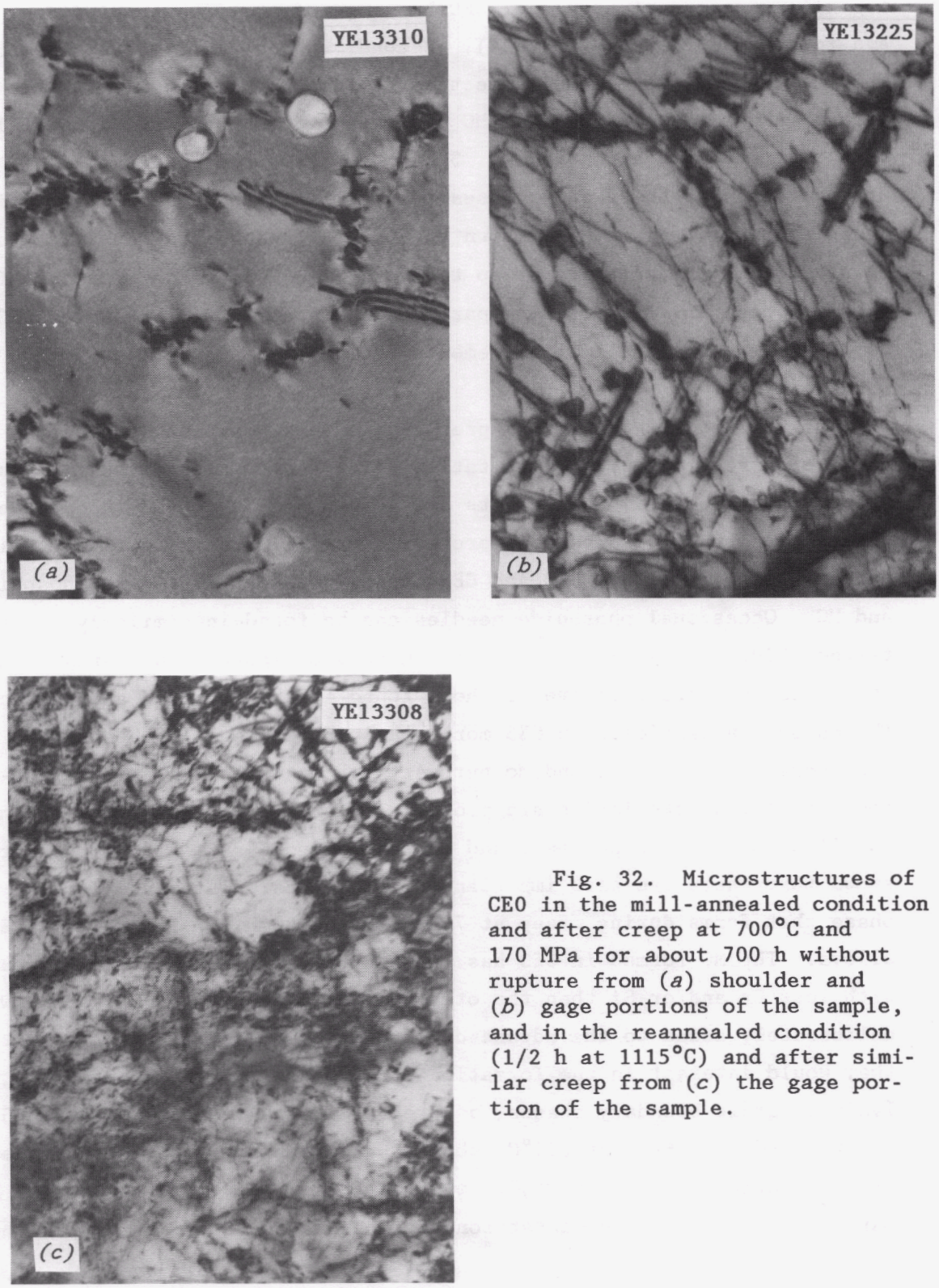

Fig. 32. Microstructures of CE0 in the mill-annealed condition and after creep at 700°C and 170 MPa for about 700 h without rupture from (*a*) shoulder and (*b*) gage portions of the sample, and in the reannealed condition (1/2 h at 1115°C) and after similar creep from (*c*) the gage portion of the sample.

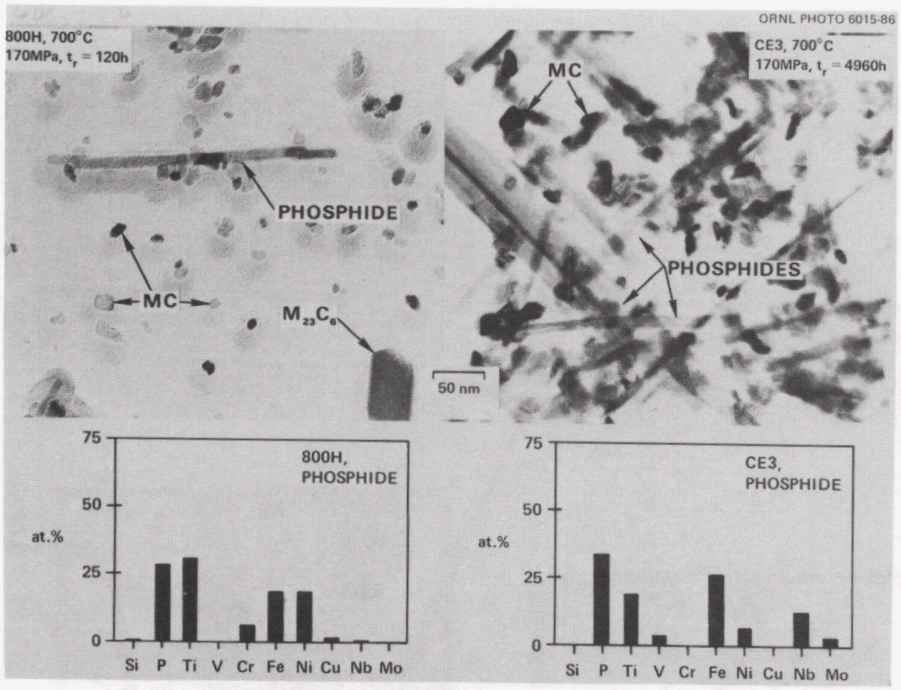

Fig. 33. Phosphide particles extracted on replicas from 800H and CE3 after creep testing at 700°C and 170 MPa. Histographs of composition determined via X-ray energy dispersive spectrocopy are included.

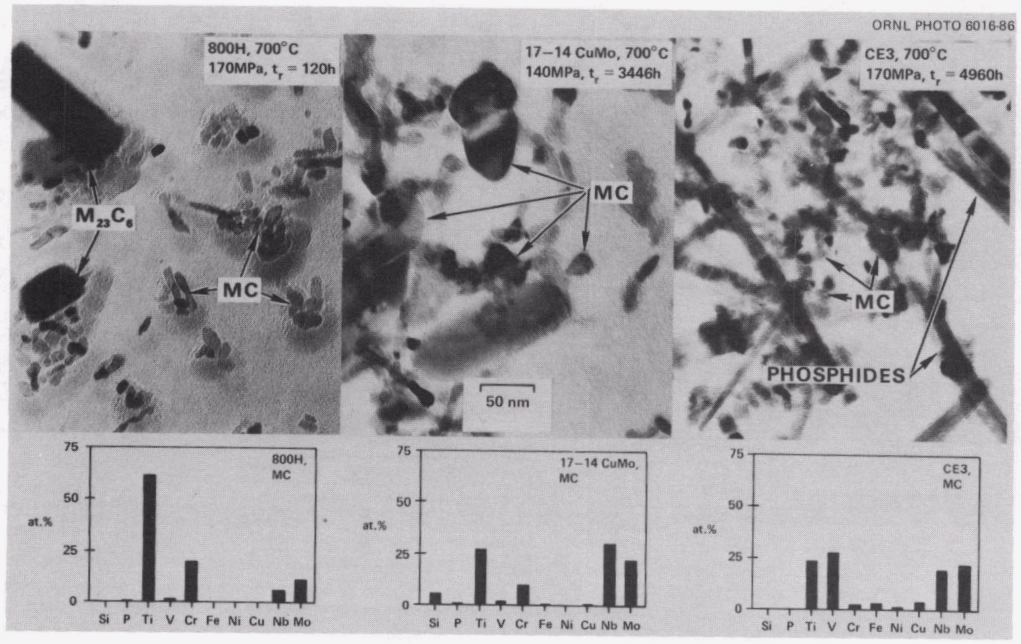

Fig. 34. MC particles extracted on replicas from alloys 800H, 17-14CuMo, and CE3 creep tested at 700°C as indicated. Histographs of composition determined via X-ray energy dispersive spectroscopy are also included.

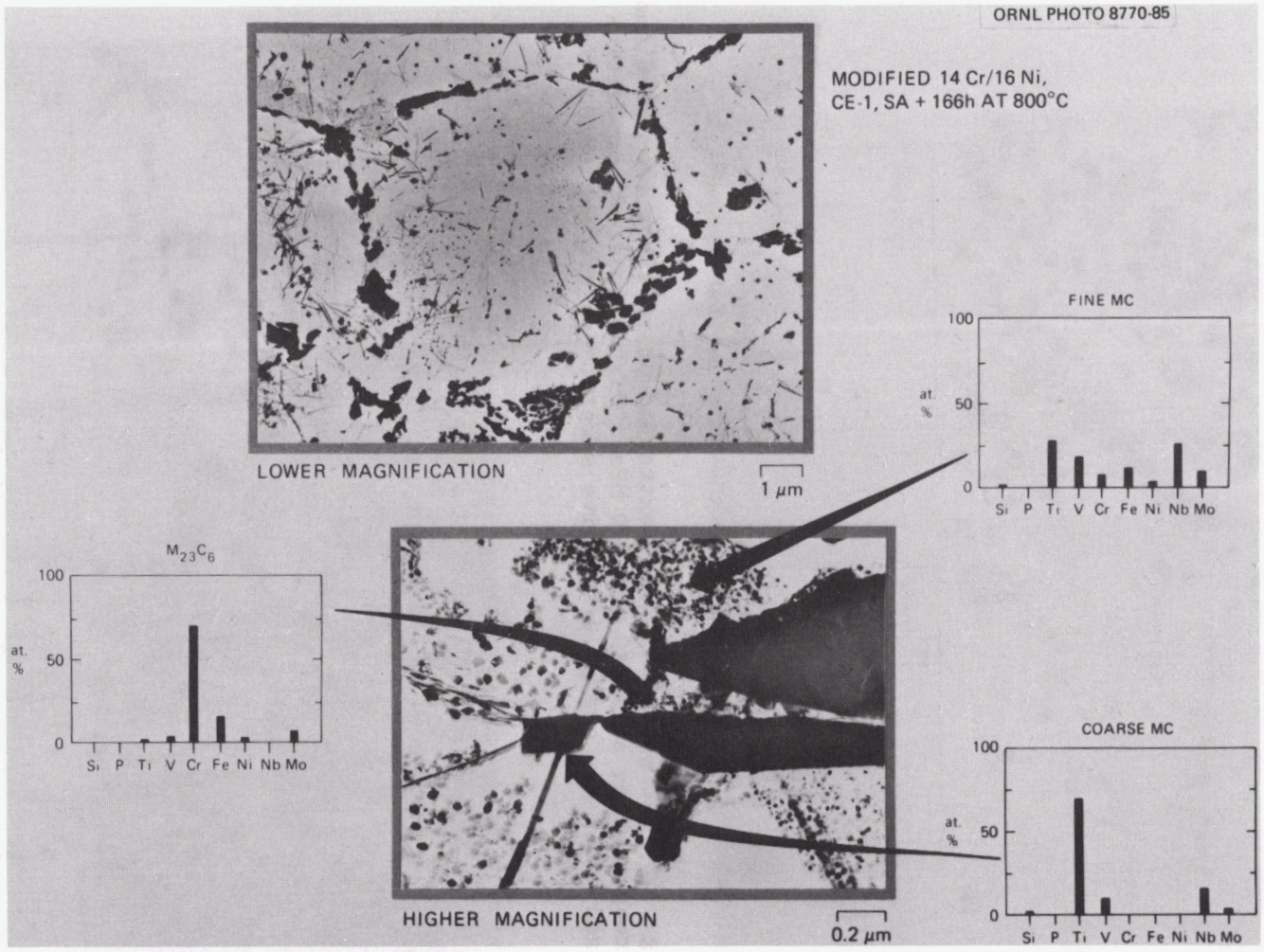

Fig. 35. Analysis of $M_{23}C_6$ and MC phases along grain boundaries on an extraction replica produced from CE1 alloy reannealed for 1 h at 1120°C and then aged for 166 h at 800°C, with histographs of phase compositions determined via X-ray energy dispersive spectroscopy.

how different the phase composition is with size, which is another important new finding of this work. Additional phases that have been identified at the grain boundaries of creep-tested CE0 and CE3 specimens include Laves (Si, Mo-rich, with Fe and some Cr), M_6C (Si, Mo, with some Cr and Fe, but more Ni than any of the other phases), phosphides, and some relatively pure Cu particles (CE3 only). Work is continuing, with large-area broad-beam XEDS analyses complementing the analysis of individual phase particles by yielding an indication of relative fractions of the various phases.

DISCUSSION

The screening tests conducted on the lean stainless steels represented by alloys CE0, CE1, CE2, and CE3 confirm expectations based upon the microstructural insight used to design the alloys. The alloys are easy to fabricate, have excellent short-time creep strength, are metallurgically stable, but are marginal with regard to weldability and have poor oxidation resistance. It has not been determined if the strengths of these alloys will last beyond 10,000 h and endure for the expected life of a superheater/reheater in an advanced steam plant. To reach any meaningful conclusion in this regard, very long testing will be necessary. Some help can be obtained from a thorough understanding of the deformation mechanisms and the extent to which the evolving substructure controls those mechanisms. However, much of this research has yet to be performed.

The examination of the 20Cr-30Ni alloys (AMAX) has not progressed to a point where their limitations have been identified. Tensile properties were found to be adequate, and the data from the creep testing at 700°C indicated that strengths equivalent to those of the lean ($\leq$14%Cr; $\leq$16%Ni) steels may not be achieved. The 20Cr-30Ni alloys appear to be substantially stronger than alloy 800H.

RECOMMENDATIONS

Evaluation of at least two alloys in the CE series of lean stainless steels should continue. One of these heats should be a copper-bearing high-phosphorus heat similar to CE3. The second heat should be similar to CE1 but with reduced phosphorus. Both heats should be of sufficient size to produce tubing of 50-mm diam and 12-mm wall thickness. Chromizing of the tubing and specimens machined from tubing should be undertaken as part of the procurement specification. Welds in tubing should be attempted. Full-size tubes, with welds, should be tested in creep rupture. Specimens subjected to weld simulation by the Gleeble should be creep tested.

The examination of the 20Cr-30Ni alloys should continue to establish the optimum annealing conditions, the weldability of the alloys, and their sensitivity to phosphorus in regard to strength and fabricability. The procurement of tubing should be delayed until this screening work is completed.

ACKNOWLEDGMENTS

Much of the testing was performed by B. C. Williams. Advice and encouragement were provided by R. R. Judkins and R. A. Bradley. Technical reviews were provided by R. L. Heestand and J. C. Griess. David Sponseller was helpful in solving some of the potential problems in alloy production. The report was edited by E. W. Whitfield and prepared for publication by D. J. Walmsley.

REFERENCES

1. P. L. Rittenhouse et al., *Assessment of Materials Needs for Advanced Steam Cycle Coal-Fired Plants*, ORNL/TM-9735, August 1985.

2. R. A. Bradley and P. T. Carlson, *Advanced Research and Technology Development Fossil Energy Materials Program Implementation Plan for Fiscal Years 1986 Through 1990*, ORNL/TM-9825, April 1986.

3. M. Gold and R. I. Jaffee, "Materials for Advanced Steam Cycles," *J. Mater. for Energy Syst.* 3, 138-45 (September 1984).

4. R. W. Swindeman et al., *Alloy Design Criteria and Evaluation Methods for Advanced Austenitic Alloys in Steam Service*, ORNL-6274, May 1986.

5. J. H. Harlow, "Metallurgical Experience with the Eddystone 5000 psi 1200 F Unit No. 1," paper 10 in *Joint International Conference on Creep*, Institute of Mechanical Engineers, London, 1975.

6. J. DeLong, Philadelphia Electric Company, to R. W. Swindeman, ORNL, private communication, 1982.

7. H. E. McCoy and J. F. King, *Mechanical Properties of Inconel 617 and 618*, ORNL/TM-9337, February 1985.

8. G. M. Goodwin, "Development of a New Hot-Cracking Test — the Sigmajig," *Weld. J.* **66**(2), 33–38 (February 1987).

9. *Creep Data Sheet No. 6a*, National Research Institute for Metals, Tokyo, 1978.

10. E. G. Wilson, "Stress Varied Creep of 20%Cr-25%Ni-Nb Stabilized Austenitic Stainless Steel," pp. 111-21 in *Creep Strength in Steel and High-Temperature Alloys*, The Metals Society, London, 1974.

INTERNAL DISTRIBUTION

1–2. Central Research Library
3. Document Reference Section
4–5. Laboratory Records Department
6. Laboratory Records, ORNL RC
7. ORNL Patent Section
8. R. A. Bradley
9. C. R. Brinkman
10. P. T. Carlson
11. D. F. Craig
12. R. S. Crouse
13. J. R. DiStefano
14–18. G. M. Goodwin
19. J. A. Horak
20. R. R. Judkins
21. J. F. King
22. R. L. Klueh
23. C. T. Liu
24–28. P. J. Maziasz
29. A. R. Olsen
30. D. F. Pedraza
31. A. F. Rowcliffe
32. A. C. Schaffhauser
33. G. M. Slaughter
34. J. O. Stiegler
35–39. R. W. Swindeman
40–42. P. T. Thornton
43. J. R. Weir
44. G. Y. Chin (Consultant)
45. H. E. Cook (Consultant)
46. F. F. Lange (Consultant)
47. T. E. Mitchell (Consultant)
48. W. D. Nix (Consultant)
49. J. C. Williams (Consultant)

EXTERNAL DISTRIBUTION

50-51. ARGONNE NATIONAL LABORATORY, 9700 S. Cass Avenue, Argonne, IL 60439

W. A. Ellingson
K. Natesan

52. AMERICAN WELDING INSTITUTE, New Topside Road, Rt. 4, Box 90, Louisville, TN 37777

J. Landes

53. BABCOCK & WILCOX, Fossil Power Generation Division, 20 South Van Buren Avenue, Barberton, OH 44203

M. Gold

54. P. M. Brister, Rt. 3, Box 3056, Carnesville, GA 30521

55. CABOT CORPORATION, Corrosion Resistant Alloys, 1020 West Park Avenue, Kokomo, IN 46901

A. I. Asphahani

56. CANADA CENTRE FOR MINERALS AND ENERGY TECHNOLOGY, 568 Booth Street, Ottawa, Ontario, Canada K1A OG1

    R. W. Revic

57. CARPENTER TECHNOLOGY CORP., Steel Division, P.O. Box 662, Reading, PA 29603

    J. W. Martin

58. CHICAGO BRIDGE AND IRON COMPANY, 800 Jorie Blvd., Oak Brook, IL 60521

    E. Upitis

59. ROBERT L. CLOUD AND ASSOCIATES, 125 University Ave., Berkeley, CA 94710

    W. R. Mikesell

60. COMBUSTION ENGINEERING, INC., 911 W. Main Street, Chattanooga, TN 37402

    D. A. Canonico

61. COMMISSION OF THE EUROPEAN COMMUNITIES, Petten Establishment, Postbus 2, 1755 ZG Petten, The Netherlands

    Marcel Van de Voorde

62. CORNELL UNIVERSITY, Materials Sciences and Engineering Department, Bard Hall, Ithaca, NY 14853

    Che-Yu Li

63-66. ELECTRIC POWER RESEARCH INSTITUTE, 3412 Hillview Avenue, P.O. Box 10412, Palo Alto, CA 94303

    W. T. Bakker
    R. I. Jaffee
    J. Stringer
    R. Viswanathan

67. EXXON RESEARCH AND ENGINEERING CO., P.O. Box 101, Florham Park, NJ 07932

    M. J. Humphries

68. FOSTER WHEELER DEVELOPMENT CORPORATION, 12 Peach Tree Hill Road, Livingston, NJ 07039

    W. R. Apblett, Jr.

69. GA TECHNOLOGIES, INC., Reactor Structural Materials Branch, Fuels and Materials Division, P.O. Box 81608, San Diego, CA 92138

    D. I. Roberts

70. GENERAL ELECTRIC COMPANY, Turbine Materials Engineering, Building 41, Room 306, 1 River Road, Schenectady, NY 12345

    R. M. Curran

71. GILBERT ASSOCIATES, INC., Morgantown Road, Green Hills, Reading, PA 19603

    R. L. Dail

72. INCO ALLOYS INTERNATIONAL, INC., P.O. Box 1958, Huntington, WV 25720

    T. H. Bassford

73. C. W. Lawton, 52 Chapman Road, West Hartford, CT 06107

74. William E. Leyda, 1192 Overlook Drive, Alliance, OH 44601

75. LUKENS STEEL COMPANY, R&D Center, Coatesville, PA 19320

    J. Gulya

76. THE METAL PROPERTIES COUNCIL, INC., United Engineering center, 345 E. 47th Street, New York, NY 10017

    M. Prager

77. NATIONAL MATERIALS ADVISORY BOARD, National Research council, 2101 Constitution Avenue, Washington, DC 20418

    K. M. Zwilsky

78. THE NATIONAL MATERIALS PROPERTY DATA NETWORK, INC., 345 East 47 Street, New York, NY 10017

    J. G. Kaufman

79. OFFICE OF NAVAL RESEARCH, Code 431, 800 N. Quincy Street, Arlington, VA 22217

    S. G. Fishman

80. STANDARD OIL, INDIANA, P.O. Box 400 - MS B-8, Naperville, IL 60540

    S. Ibarra

81. STONE AND WEBSTER ENGINEERING CORPORATION, 245 Summer Street, P.O. Box 2325, Boston, MA 02107

M. P. Berardi

82. SUPERIOR TUBE COMPANY, P.O. Box, 191, Norristown, PA 19404

C. C. Mathews

83. TENNESSEE VALLEY AUTHORITY, W9A61 C-K, 400 West Summit Hill Drive, Knoxville, TN 37902

M. N. Bressler

84. TENNESSEE VALLEY AUTHORITY, Metallurgical & NDT Section, 820 Chestnut Street, Tower II, Chattanooga, TN 37401

S. O. Hilton

85. R. D. THOMAS AND COMPANY, INC., 103 Avon Road, Narberth, PA 19072

R. D. Thomas, Jr.

86. U. S. STEEL CORPORATION, Room 1741, 600 Grant Street, Pittsburgh, PA 15230

C. E. Spaeder

87-88. UNIVERSITY OF CALIFORNIA AT BERKELEY, Department of Materials Science and Mineral Engineering, Berkeley, CA 94720

E. R. Parker
R. O. Ritchie

89. UNIVERSITY OF CALIFORNIA AT SANTA BARBARA, Department of Chemical and Nuclear Engineering, Santa Barbara, CA 93106

G. R. Odette

90. UNIVERSITY OF ILLINOIS, Department of Mechanical and Industrial Engineering, 1206 W. Green Street, Urbana, IL 61801

D. L. Marriott

91. UNIVERSITY OF MANCHESTER INSTITUTE OF SCIENCE AND TECHNOLOGY, P.O. Box 88, Manchester, M601QD, United Kingdom

F. H. Stott

92. UNIVERSITY OF PITTSBURGH, Department of Metallurgical and Materials Engineering 848 Benedum Hall, Pittsburgh, PA 15261

G. H. Meier

93. UNIVERSITY OF SOUTHERN CALIFORNIA, Department of Materials Science, Los Angeles, CA 90089

J. A. Todd

94. UNIVERSITY OF TENNESSEE, Department of Materials Science, Knoxville, TN 37996

C. D. Lundin

95. WESTINGHOUSE ELECTRIC CORPORATION, Research and Development Center, Westinghouse Building, Gateway Center, Pittsburgh, PA 15222

B. J. Shaw
S. C. Singhal

96. DOE, ENERGY CONVERSION AND UTILIZATION TECHNOLOGIES DIVISION, CE-14, 5E-091 Forrestal Building, Washington, DC 20585

J. J. Eberhardt

97. DOE, OAK RIDGE OPERATIONS OFFICE, P.O. Box E, Oak Ridge, TN 37931

Assistant Manager for Research and Development

98. DOE, OFFICE OF BASIC ENERGY SCIENCES, Materials Sciences Division, ER-131, J314/GTN, Washington, DC 20545

F. V. Nolfi, Jr.

99-100. DOE, OFFICE OF FOSSIL ENERGY, Washington, DC 20545

J. P. Carr (FE24, C179/GTN)
R. E. Harrington (FE-20, C164/GTN)

101. DOE, OFFICE OF VEHICLE AND ENGINE R&D, CE-131, 5G-064 Forrestal Building, Washington, DC 20585

R. B. Schultz

102-105. DOE, MORGANTOWN ENERGY TECHNOLOGY CENTER, P.O. Box 880, Morgantown, WV 26505

J. W. Byam, Jr.
D. Dubis
J. E. Sholes
J. S. Wilson

106-109. DOE, PITTSBURGH ENERGY TECHNOLOGY CENTER, P.O. Box 10940, Pittsburgh, PA 15236

R. A. Carabetta
S. W. Chun
J. J. Joubert
F. W. Steffgen

110-139. DOE, TECHNICAL INFORMATION CENTER, P.O. Box 62, Oak Ridge, TN, 37831

For distribution by microfiche as shown in DOE/TIC-4500, Distribution Categories UC-90e (Direct Combustion of Coal) and UC-90H (Materials and Components).

☆ United States Government Printing Office: 1987—748-168/60021